Carbon Backsputter Mitigation with a Cusped Field Retarding Beam Dump

IEPC-2025-417

Presented at the 39th International Electric Propulsion Conference, Imperial College London, London, United Kingdom
14-19 September 2025

Braden Oh* Andrew Schok† Christopher McCullough‡ William Hurley§ Collin Whittaker¶
Tate Gill‖ Thomas Marks**Benjamin Jorns††
University of Michigan, Plasmadyamics and Electric Propulsion Laboratory, Ann Arbor, MI, 48105

The ability to electrostatically decelerate thruster beam ions as a means of reducing carbon backsputter in an electric propulsion test facility is experimentally evaluated. Previous work has shown that while this type of ion-decelerating 'beam catcher' may reduce backsputter, it can confound deposition measurements by launching high-energy ions back at the thruster. This study evaluates the effectiveness of canting the beam catcher in an effort to redirect backstreaming ions away from the thruster. The efficacy of this technique is evaluated by measuring the reduction in backsputter deposition/ion-induced erosion in the plane of the thruster with an electrostatically filtered quartz crystal microbalance (QCM). It is found that canting the beam catcher reduces the magnitude of backstreaming ion erosion by 64% when canting the beam catcher up to 27° with respect to thruster centerline at a fixed bias of 150V and by 77% when canting the beam catcher up to 33° at a fixed bias of 125V. While negative backsputter rates were not completely eliminated, it is shown through QCM data and a test employing grounded witness plates that this persistent erosion may be explained by the presence of low-energy background ions eroding material from grounded surfaces. Key challenges and limitation in the experimental configuration, particularly the use of a "guarded QCM" are discussed. The implications of these findings and future avenues for probing and scaling beam catcher concepts are examined in the context of establishing ground-based high fidelity test environments.

I. Introduction

Backsputter of facility material poses a major challenge to the testing and flight-qualification of high power electric propulsion systems. This process is characterized by the sputterants from the walls of a test chamber bombarded by the thruster ion beam returning to coat the thruster. The resulting material accumulation is particularly problematic for flight qualification tests where a primary goal is to evaluate the erosion rate of life-limiting components (e.g. Hall thruster pole cover erosion[1–4] or gridded ion thruster accelerator grid erosion[5]). To date, this problem has largely been addressed through computational modeling.[6,7] However, these techniques are limited when characterizing higher power systems in which backsputter deposition can dominate and obscure the erosion process,[4,8] rendering the experimental deconvolution of backsputter and erosion rates impossible.

With this limitation of present techniques in mind, we have explored the possibility of reducing backsputter production by decelerating thruster ions electrostatically before striking the facility boundaries. In an

*Ph.D. Candidate, Department of Aerospace Engineering. bradenoh@umich.edu
†MSE Student, Department of Aerospace Engineering.
‡MSE Student, Department of Aerospace Engineering.
§Ph.D. Candidate, Department of Aerospace Engineering.
¶Research Scientist, Department of Aerospace Engineering.
‖Research Scientist, Department of Aerospace Engineering.
**Postdoctoral Research Fellow, Department of Aerospace Engineering.
††Associate Professor, Department of Aerospace Engineering.

optimal configuration, the ions would be decelerated to below the sputter threshold of the beam dump material, completely eliminating backsputter at the source. We have shown that in order to maintain sufficient decelerating voltage in a Hall thruster plume, it is necessary to use a combination of a positively biased plate (with respect to the thruster) and a transverse magnetic field in front of the plate. The magnetic field serves to reduce parasitic electron current which, when unimpeded, precludes the ability to maintain sufficiently high decelerating voltages.

In previous efforts, these types of magnetically-assisted retarding beam dumps have been tested at small scale. One placed in the far field of a gridded ion thruster supported bias voltages up to 600V.[9] Another placed in the near field of a 4.5 kW Hall thruster plume exhibited floating voltages up to 40V, but experienced strong electrical coupling to the thruster that precluded active biasing.[10] In a follow on effort,[11] we demonstrated that in the far field of a 4.5 kW Hall thruster discharge, a highly biased beam dump did not majorly perturb thruster operation: thrust, anode current oscillations, and plume potential in the near field all remained unchanged at biases in excess of 150V. While the plume current distribution did vary at large oblique angles with decelerating voltage, we concluded that this was likely due to a secondary effect of increasing neutral density rather than the electrical configuration of the beam dump.

Although these prior studies showed that a prototype-scale magnetically-assisted retarding beam dump can provide retarding biases while minimally affecting thruster operation, we found evidence of an unintended secondary effect: backstreaming energetic ions toward the thruster. We hypothesized these arose primarily from charge exchange ions accelerated away from the beam dump with energy commensurate with the decelerating voltage. This effect rendered us unable to deconvolve the effects of ion erosion and reduction in carbon deposition on the measured net backsputter rate in the plane of the thruster. Despite then the promising potential of the beam dump configuration, the need is apparent for a detailed study of these backstreaming ions. Our dual goals include identifying strategies to mitigate this effect near the thruster and in so doing quantify the effectiveness of the retarding beam dump at reducing carbon backsputter.

To this end, this paper is organized in the following way. In Section II we explain the principles of operation of the magnetically assisted retarding beam dump and describe the challenge of and possible mitigation for backstreaming ions. In Section III we describe the design of our experimental apparatus, a cusped magnetic field beam dump on rotation stages. In Section IV we describe our experimental configurations. In Section V we relate the diagnostic tools we employ. In Section VI we present the results of our experiments. In Section VII we discuss the implications of our findings with respect to minimizing backstreaming ion erosion and carbon backsputter reduction.

II. Theory of Operation

In this section, we explain the principles of operation for the magnetically-assisted ion retarding beam dump, hereafter referred to as a 'beam catcher.' We first describe the technique of reducing ion energy electrostatically and explain the need for an magnetic field. We conclude with a discussion of the backstreaming ion problem and how canting the beam catcher plate may serve as a mitigation.

A. The need for ion energy reduction to reduce backsputter

Beam dumps typically consist of flat plates placed downstream of a thruster ion beam, often canted or otherwise arranged in a way to improve pumping speeds.[12] High-energy ions that bombard these plates sputter material from the surface that subsequently recondenses elsewhere in the facility. To reduce the rate of backsputter (and correspondingly, the erosion rate of the beam dump), beam dumps are typically made from a material with a low sputter yield, such as graphite.

The sputter yield of the material (e.g. Figure 1) is a nonlinear function of ion energy.[13] As a result of this dependence, reducing the energy of bombarding ions can lead to disproportionate reduction in sputtered material. For example, for a Hall thruster operating at 300V potential,[8] reducing beam energy by 50% (i.e. a 150 V retarding potential) could yield a backsputter reduction of 84%. In principle, it is even possible to entirely eliminate sputtering by lowering the incident energy below the sputter threshold energy for the beam dump material (for xenon ions bombarding graphite, this energy is predicted to be approximately 21V[14]). With this motivation in mind, we review in the following our method for reducing the energy of incident ions.

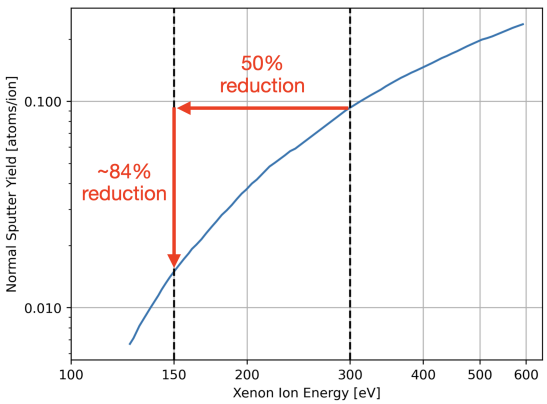

Figure 1: Sputter curve for graphite oriented normal to a xenon ion beam as reported by Williams et al.[13] The vertical lines at 300 eV and 150 eV illustrate how a 50% reduction in ion energy can yield a disproportionate reduction in backsputter.

B. The need for a cross-field configuration

To attain reductions in ion energy sufficient to mitigate backsputter, our technique is to electrostatically decelerate beam ions prior to striking the beam dump. As we have discussed in Ref. 11, we achieve this effect in the plume of the Hall thruster by employing an electrically biased graphite plate with a transverse magnetic field (Fig. 2b). The magnetic field is necessary to attenuate electron current to the beam dump and thereby electrically de-couple the beam dump bias from the main discharge (Figs. 2a and 2c). We have shown in previous work that this type of "beam catcher" can sustain high bias voltages[9] while minimally affecting thruster operation.[11]

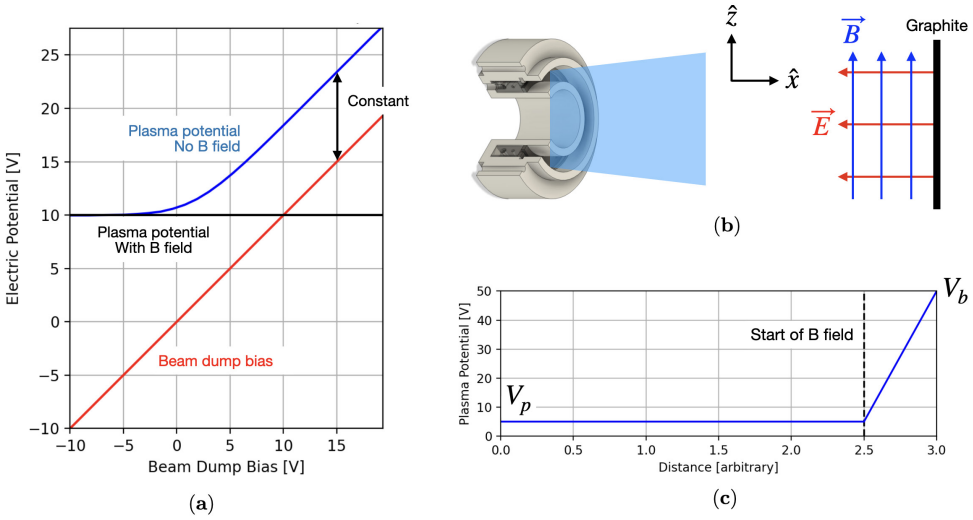

Figure 2: Notional illustrations of (a) plasma potential vs. beam dump bias without a magnetic field (blue) and with a magnetic field (black), (b) the beam catcher field geometry, and (c) the notional plasma potential as a function of distance (assuming a constant magnetic field). In (c) V_p and V_b represent plasma plume potential and plate bias potential, respectively.

C. The problem of and proposed solution to backstreaming ions

We have implemented versions of a magnetized beam dump in two previous studies. While both studies indicated that the backsputter from the facility were likely reduced with these systems, we also found that the beam catchers were likely a source of high-energy backstreaming ions. We believe that these ions sputtered material from surfaces near the thruster, thereby driving "negative" deposition rates as measured by sensors at the thruster plane.[9,11]

We illustrate a possible process for formation of these backstreaming ions in Fig. 3a. High energy ions from the thruster (1) decelerate, strike the beam dump plate, and are neutralized. These slow moving neutrals undergo charge exchange with incoming high speed ions (2) near the plate and are launched back at the thruster (3), accelerating through the a substantial fraction of the potential difference between the bias plate and the plasma beam (4).

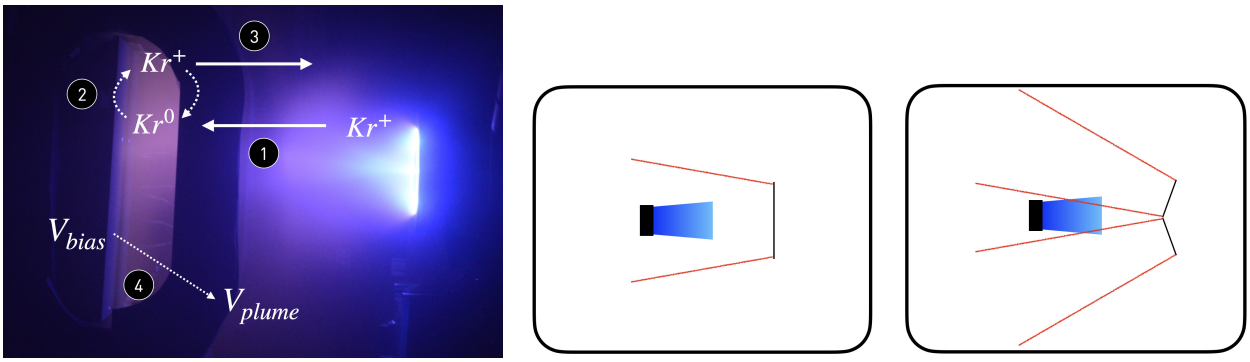

(a) (b) (c)

Figure 3: Notional illustrations of the process by which high energy ions may be backstreaming to the thruster with (a) Backstreaming ion production, b) Characteristic divergence of a backstreaming ion beam, and c) Backstreaming ion mitigation by canting the beam catcher

Given that the electric potential of the beam catcher is largely normal to its surface, this formation process would imply that the backstreaming ions have a characteristic divergence angle emerging from the beam dump (Figure 3b) . This invites the possibility that the configuration may be canted in such a way to minimize the degree to which backstreaming ions return to the the actual thruster. Figure3c illustrates, for example, how a wedge-shaped beam catcher with a cant angle greater than this characteristic divergence angle could, in principle, create an ion-free window down the centerline of the wedge.

Having established the principles by which we seek to reduce backsputter and minimize the effect of backstreaming ion erosion, we now proceed to describe the experiments we performed to evaluate the effectiveness of the beam catcher at reducing carbon backsputter and of canting the beam catcher to mitigate backstreaming ion erosion.

III. Beam Catcher Design

In this section, we describe our approach to designing and performing a study of a facility-scale beam catcher in the plume of a Hall effect thruster. We introduce the cusped magnetic field beam catcher we designed for this study and describe the software tools we used to optimize the placement of the beam catcher in the facility. We then overview the actuation system, facility, and thruster we employed for this study.

A. Magnetic field configuration

In our previous work,[11] we adopted a solenoid-configuration to provide a transverse magnetic field to a graphite plate. While we were ultimately able to demonstrate that this configuration could reduce backsputter, the solenoids–which encircled the bias plates–were a source of sputtering that would become more severe with cant angle. To overcome this limitation, we adopted a cusped magnetic field generated by a set

of magnetic rails of alternating polarity located behind the bias plate (Figure 4). In this way, we entirely hide the magnetic field-generating components from the incident beam, effectively eliminating the magnetics as a source of backsputter.

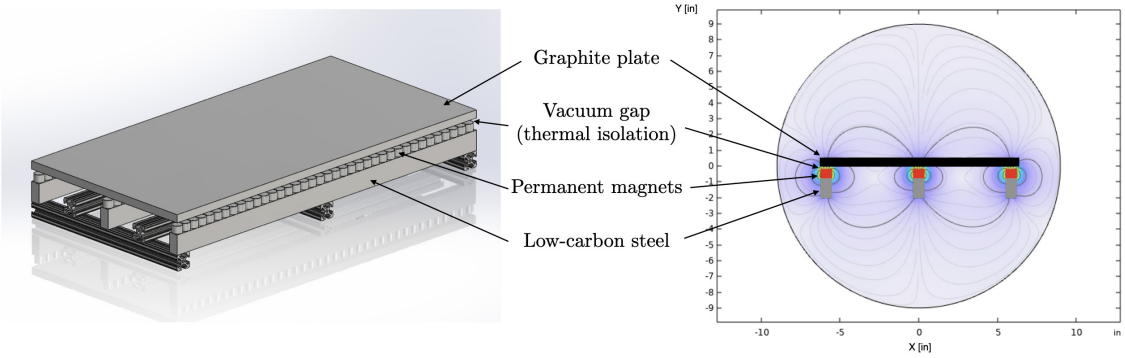

(**a**) (**b**)

Figure 4: Mechanical design of the cusped field beam catcher showing (a) CAD prototype assembly and (b) Corresponding magnetic field shape simulated using COMSOL Multiphysics.

To generate the field, we constructed rails of 2.54 cm cube N52 grade neodymium magnets magnetically attached to a 1018 grade low-carbon steel bar to enhance field strength. Three rails were spaced approximately 30 cm apart behind a graphite bias plate measuring 0.61 × 1.22 m. The center rail had opposite polarity from the outer rails so as to create a magnetic field with two cusps, as shown in Fig. 4. We maintained a 64 mm vacuum gap between the graphite plate and magnet rails to thermally isolate the magnets from the deflector plate. This is significant because the N52 magnets we employed have a maximum operating temperature of only 80°C. Although the Curie temperature for neodymium magnets is generally on the order of 300°C, the magnetic properties of individual magnets (e.g. field strength and orientation) begin to vary from specification at much lower temperatures. This onset is determined by the material composition and manufacturing process and is reported by the manufacturer as a maximum operating temperature.

The right panel of Fig. 4 shows a simulation of this configuration generated with COMSOL Multiphysics. We verified these simulation results after assembly with a Gauss meter, the results of which are shown in Fig. 5. The peak magnetic field strength between magnetic rails is 143 G at a height of 5 cm above the surface of the bias plate. The maximum field strength at the outer cusp is 534 G and at the inner cusp is 849 G. This facilitates magnetic mirroring of electrons and thereby reduces the amount of electron current drawn into the bias plates in order to apply large biases.

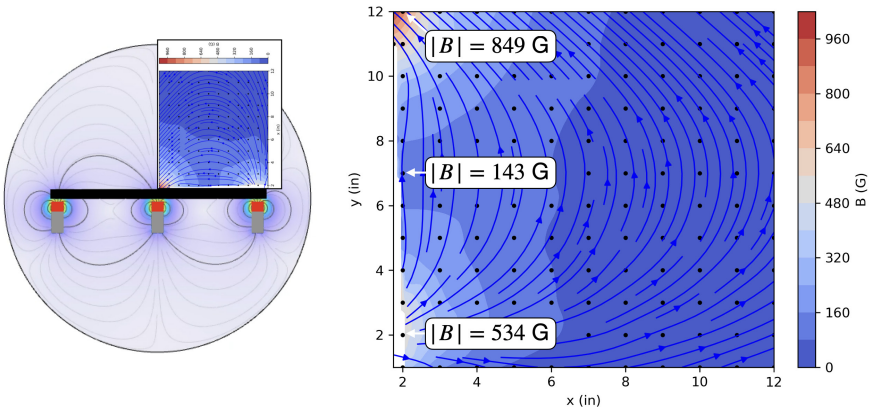

(**a**) (**b**)

Figure 5: Magnetic field map illustrations showing (a) Where the magnetic field map of the beam catcher was taken and (b) The resultant field map. Locations where data were taken are marked by black dots and the contour plot was generated by interpolation.

We placed electrically floating grafoil strips on the surface of the bias plate at the magnetic cusps (i.e. over the magnetic rails). These strips were 2.54 cm wide (the same width as the magnets behind them) and were electrically isolated from the bias plate by fiberglass tape. We adopted this configuration to further reduce the electron current that could escape through the cusps to the beam catcher plate.

B. Rotation stages

We constructed two cusped-field beam catchers per the above description and placed them side-by-side, angled in opposite directions to form a wedge along thruster centerline. Figure 6 shows photographs of the assembled beam catcher with support structures and actuation hardware. Assuming that backstreaming ions exhibit a characteristic divergence angle emerging from the beam dump, selecting a wedge angle greater than this divergence angle could, in principle, create a window at the thruster that is free of backstreaming ions (Figure 3c).

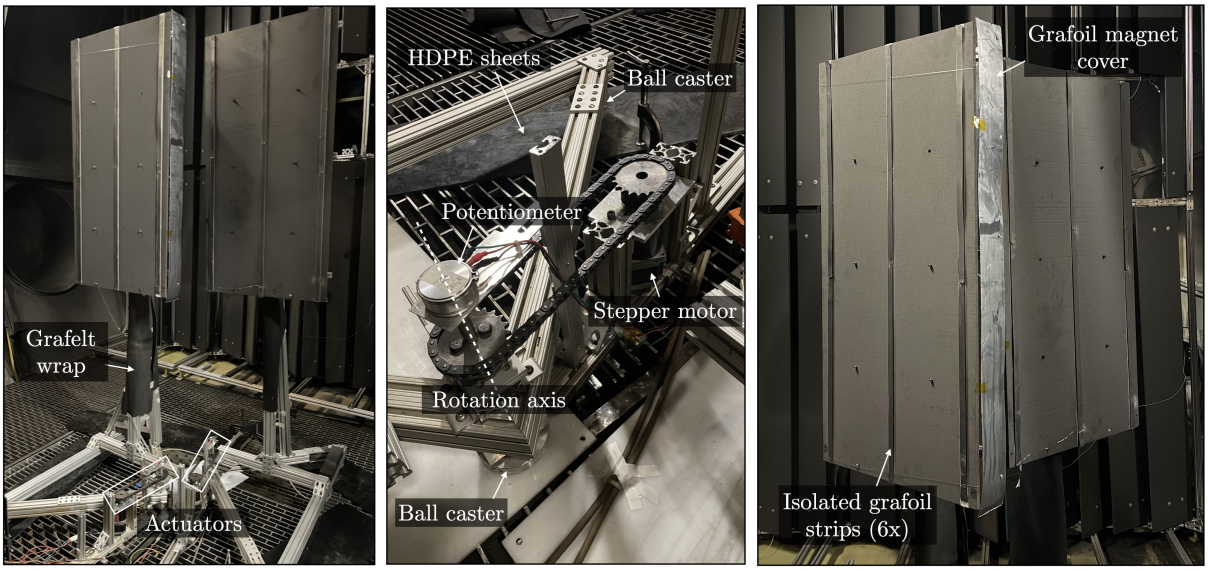

(a) (b) (c)

Figure 6: Photographs of the cusped-field beam catcher (a) Full tower assembly, (b) Actuation system (for the rear tower), and (c) View from the thruster at full cant.

We built support structures for each tower on top of ball casters. We in turn attached a motor to each support structure using a gear and chain. The pivot point for each tower was directly under the center-most edge of the deflector plate, enabling the towers to be actuated along the center of the wedge. We measured the angle of each tower using potentiometers fixed to each pivot point. The geometry of the support bases limited the maximum cant angle to 40° for each tower. We wrapped the metal surfaces of the support frame exposed to the thruster beam in grafelt to minimize backsputter. We covered the surface of the bias plate above the magnet rails with grafoil covers that were electrically isolated from the bias plate with fiberglass tape.

In the implementation inside the test facility, we staggered the beam catcher panels by placing one tower 30 cm behind the other. We elected to use this configuration because placing the panels directly side by side in a wedge shape centered on the thruster would result in an electric field pointed directly back at the thruster along the centerline of the wedge, thereby directing centerline ions back to the thruster. Staggering the beam catcher panels would superimpose the two towers' electric fields in such a way to direct centerline ions away from thruster centerline, in the direction of the rear tower's cant.

C. Placement with respect to thruster

To identify the placement of the beam catcher in the facility that would most significantly reduce backsputter, we performed carbon deposition simulations using the *Sputterer* code developed by Marks.[15] *Sputterer* is a

GPU-accelerated Monte Carlo particle transport code designed to track the the sputtering and deposition of carbon atoms originating from surfaces in contact with energetic plasma plumes, like those commonly seen in EP systems. It models plume interactions with arbitrary 3D geometries and is designed to provide fast, moderate-fidelity estimates of carbon back-sputtering, making it well-suited for rapid design optimization for EP testing applications. Further details on the simulation configurations we used are given in Appendix A. Figure 7 shows screenshots from a *Sputterer* simulation of a thruster firing at a passive beam dump.

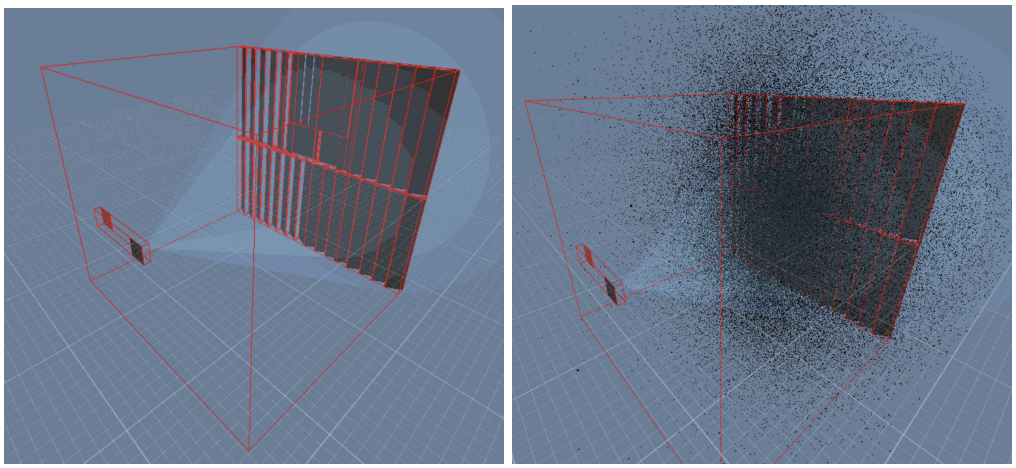

(a) (b)

Figure 7: Example outputs of *sputterer* simulation of a passive beam dump showing (a) Plume profile and boundary boxes and (b) An active backsputter simulation.

We performed two sets of simulations. In the first, we explored the effects of cant angle and introducing a gap between the towers, details of which are provided in Appendix A. These studies showed that backsputter is minimized by having no radial gap between the towers and using a cant angle of 0°, so as to maximize the cross sectional area of the bias plate exposed to the ion beam. The practical implication of this is that the beam catcher should utilize the shallowest cant angle necessary to mitigate backstreaming ions.

Our key objective for the second set of simulations was to evaluate how the distance from the thruster (hereafter referred to as the *range*) affects deposition rates at the thruster. This is significant because for a fixed divergence angle of backstreaming ions, a steeper cant angle would be required at short ranges than at long ranges to deflect ions away from the thruster. These steeper angles have the effect of reducing the cross sectional area of the beam catcher, thereby reducing the fraction of the beam that is subtended. Although longer ranges reduce the cant angle needed for backstreaming ion mitigation, they also reduce the fraction of the beam subtended by the beam catcher and thereby increase backsputtering from the downstream facility. To investigate the balance of these effects, we used simulations to seek an optimal range at which to place the beam catcher in our experiment. In simulation, we swept the beam catcher's range and calculated at each range the cant angle required to establish a 61 cm ion-free window at the thruster, assuming a backstreaming ion divergence angle of 18°. Figure 8a illustrates the beam catcher variables in the context of simulation geometry. Because this simulation sought only to compare *relative* backsputter production rates, the width of the ion free window and the divergence angle were arbitrary parameters. The width we selected was approximately twice the width of our thrust stand; the divergence angle was physically (but inconclusively) motivated by unpublished data we took after the conclusion of Hurley.[10] Figure 8b shows the results of these simulations. An optimal range of 1.6-1.8 m is readily apparent.

Taken together, these simulations demonstrated that backsputter minimization will occur when the beam catcher is located 1.6-1.8 m downstream of the thruster, with no radial gap between the towers, and using the shallowest cant angle needed to mitigate ion backstreaming. Armed with these insights, we describe in the next section the experimental implementation and key results from the wedge and canted beam catcher.

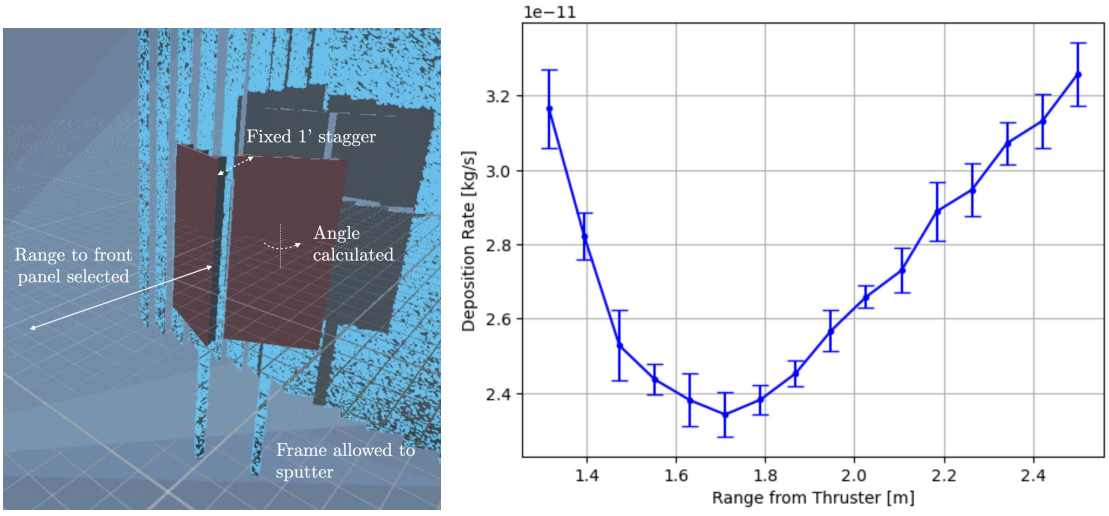

(a) (b)

Figure 8: Beam catcher simulation results showing (a) the physical configuration in the simulation and (b) the results of simulating deposition as a function of range assuming 18° divergence.

IV. Experimental Setup

In this section we describe the experimental setups we used in this work. First, we describe the test facility, thruster, and thruster operating conditions we used. This is followed by the configuration of test articles and probes in the facility across the two individual studies we performed.

A. Facility and thruster

We used the HCDv2 magnetically-shielded laboratory Hall thruster operating on argon as the ion source for these tests. The HCDv2 is the second iteration of a laboratory Hall thruster developed by the University of Michigan as a part of the DARPA Thruster Advancements for Low-altitude Operations in Space (TALOS) research program. We operated the HCDv2 on argon at 2 kW (200V, 10A) of discharge power in these tests. The discharge chamber in this device is comprised of boron nitride, the anode of stainless steel, and the magnetic pole covers of graphite. It employs an externally mounted heaterless lanthanum hexaboride (LaB_6) hollow cathode which we operated on krypton gas. We chose to use argon in order to maximize the backsputter signal to our QCM, as argon sputters carbon at higher yields than other typical propellants such as xenon and krypton.[16] We conducted all experiments inside the Alec D. Gallimore Large Vacuum Test Facility (LVTF) chamber at the University of Michigan. LVTF measures 6 m in diameter by 9 m in length and employs nineteen cryopumps to achieve a measured pumping speed of 600,000 L/s for krypton. Before taking any measurements, the thruster was allowed to run continuously at 2 kW argon for 30 minutes to reach thermal steady state.

B. Test configuration

Figure 9 shows a top-view diagram of the two setups we employed in the experimental study.

As can be seen, in both studies, we measured the backsputter rate at the thruster plane using a 'guarded QCM' (Sec. V.C). We also employed a Langmuir probe (LP) (Sec. V.A), and retarding potential analyzer (RPA) (Sec. V.B) in the thruster plane. The parameters we varied during the experiment were beam catcher bias and tower cant angle, with both towers being canted the same amount.

In the first study (Fig. 9a), we placed the LP, RPA, and QCM in a vertical stack directly above the thruster (all probes located along thruster centerline) (Fig. 10a) and employed a second RPA on a rotating arm to collect radially directed ion energy measurements. We began this study by fixing the plate bias to 150V and sweeping cant angle. Identifying a minimum in ion erosion at 27°, we then fixed the cant angle to 27° and swept plate bias.

In the second study (Fig. 9b), we placed the LP, RPA, and QCM in a vertical stack to the side of the thruster corresponding to the forward beam catcher tower (Fig. 10b). We did this to investigate whether ion backstreaming along thruster centerline (see Sec. III.B for discussion on the staggering of the segments) causes "cleaning" of probe surfaces. We also added an array of witness plates, details of which are given in Sec. V and forwent the angular RPA measurements. We began this study by fixing the bias plate to 125V in order to keep the cathode to ground voltage below 20V and swept cant angle. Observing our QCM signal diminish in strength with increasing cant angle, we proceeded to sweep the plate bias voltage at a fixed angle of 0° in order to maximize the signal to the QCM.

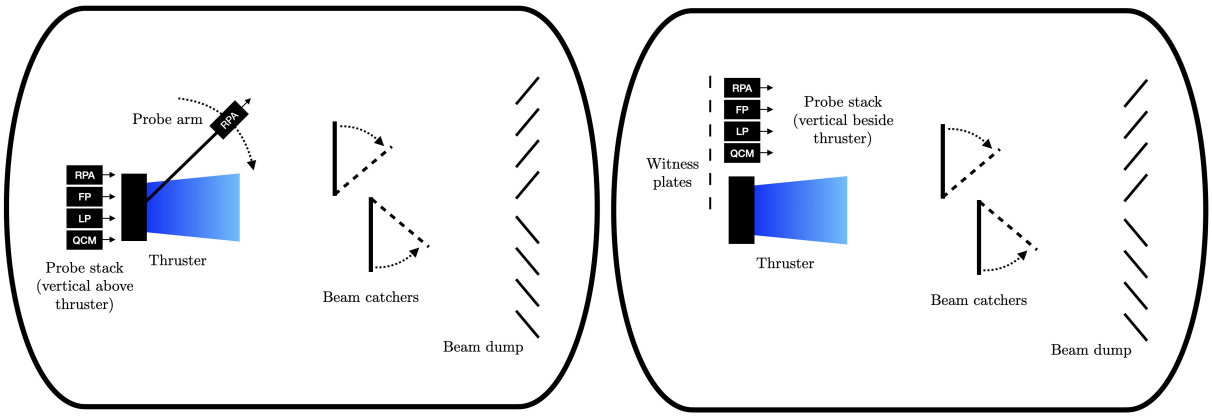

(a) (b)

Figure 9: Notional top view diagrams of the experimental configurations used in (a) Study 1, and (b) Study 2.

Table 1 gives a summary of key parameters between the two tests. The difference in ranges was due the beam catchers being uninstalled and reinstalled between studies.

	Study 1	**Study 2**
Forward tower range [m]	1.65	1.79
Rear tower range [m]	1.94	2.12
Maximum cant angle [deg]	40	34
QCM location [cm]	28 above thruster	26 beside thruster
Probe arm RPA range [m]	1.09	N/A
Witness plates present	No	Yes

Table 1: Summary of key parameters between the two studies conducted in this work.

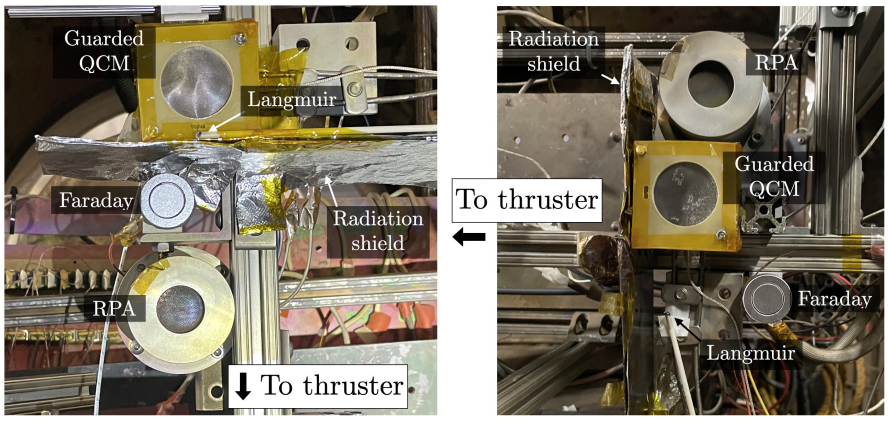

(a) (b)

Figure 10: Photographs of the probe stacks used in (a) Study 1, probes above thruster, and (b) Study 2, probes beside thruster.

V. Diagnostics

The objective of these studies was to characterize backsputter rate independent of backstreaming ion erosion and to observe the effect of cant angle as a mitigation for ion backstreaming. To characterize the far field plume of the beam catcher, we employed an array of probes facing the beam catcher to measure plasma properties near the thruster as a function of cant angle and bias voltage (Figs. 9 and 10). In this section we describe the diagnostic tools we employed and the methods of analysis for that data.

A. Langmuir probe

To measure the plasma potential near the QCM, we employed a cylindrical Langmuir probe mounted parallel to the direction of the thruster beam (and thus parallel to the backstreaming ion flow) (See Figs. 10a and 10b). As show in the example results in Figure 11, we obtained a current-voltage trace by sweeping probe voltage, V, and recording the corresponding current, I. We then inferred the plasma potential, V_p, subject to an estimate in uncertainty by using the Markov Chain Monte Carlo (MCMC) sampling inference algorithm to learn the parameters of two lines fit to the inverse temperature and electron saturation regions of the probe trace and computing the intersection of the lines. This analysis procedure is detailed in Appendix B.

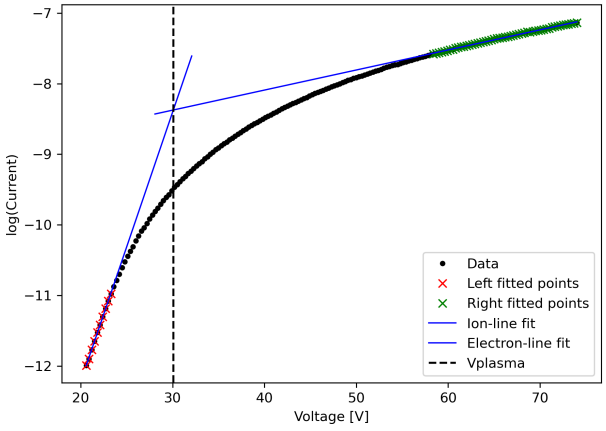

Figure 11: Prepared LP trace and line fits to the data. This data was taken at a plate bias of 125V and a cant angle of 27° and the lines shown use the mean value for each set of slope and y-intercept samples. The intersection of the lines corresponds to the 'knee' in the curve, V_p.

B. Retarding potential analyzer

To measure the energy distribution of backstreaming ions, we employed a four-grid retarding potential analyzer, an instrument which measures ion current while using a stack of conductive grids to filter ions by energy level. The first grid is allowed to electrically float and serves to attenuate plasma density in the probe. The second grid is biased to -30V to repel electrons, allowing only ions to continue through. The third grid is the ion filtering grid; its bias is swept from 0-300V and repels all ions below the filtering bias. The fourth grid is biased to -30V to suppress effects of secondary electron emission at the collector. The collector is biased to -5V and collects the ions which successfully pass through the filtering bias.

An RPA measurement is taken by measuring collector current while sweeping the filtering grid bias. Fig. 12 shows an example of this telemetry from our campaign. We extracted from this data the most probable energies of low- and high-energy populations of ions with uncertainty by fitting a dual error function to the raw probe trace using MCMC sampling. The analysis procedure for this as well as uncertainty analysis is detailed in Appendix C. An example fit of the dual error function to RPA data is shown in Fig. 12.

We note that in both experimental configurations, we employed a fixed RPA at the thruster plane, facing the beam catcher. In Study 1, we employed a second RPA on a mobile arm that was swept through the plume of the Hall thruster. This RPA was mounted facing away from the thruster so as to measure the characteristics of ions directed radially back at the thruster.

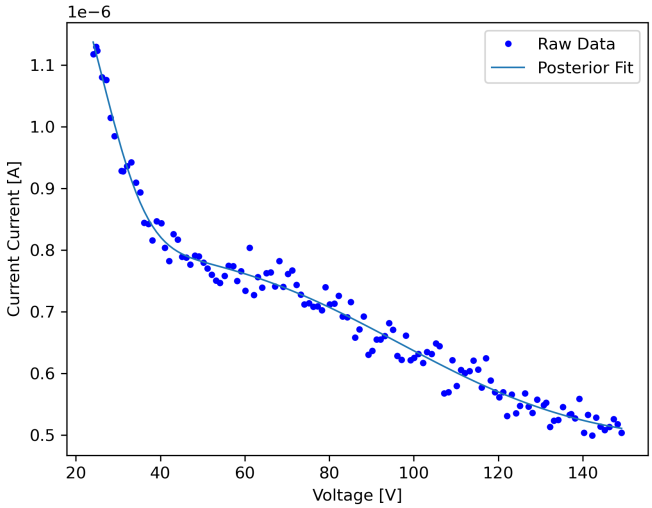

Figure 12: Raw RPA trace and dual error function fit to the data. This data was taken at a plate bias of 125V and a cant angle of 20° and the curve shown uses the mean value for each of the seven fit parameters.

C. Guarded quartz crystal microbalance

To characterize the net deposition rate at the thruster plane, we employed a quartz crystal microbalance, an instrument that measures the resonant frequency of a quartz crystal over time. To obtain a mass deposition rate, we converted frequency to film thickness using the Z-match equation developed by Lu and Lewis[17] and recorded film thickness at a 1 Hz sample rate over 15-20 minute recording windows. At a constant operating condition the film thickness is linear, so to compute backsputter rate we fit a line to the film thickness data (cf. Fig. 14). QCMs are sensitive to changes in temperature, so we employed passive liquid cooling and a radiation shield between the QCM and the thruster to maintain the QCM within 1-2°C, a range we previously observed to have a negligible effect on deposition measurements.[10]

In previous studies, we used a bare QCM to measure carbon deposition rates at the thruster. However, the QCM measures the combined effect of carbon deposition and backstreaming ion erosion, allowing for the negative *net* deposition rates previously observed.[9,11] For this reason, the effect of the beam dump on carbon backsputter alone could not be determined.[11] To overcome this limitation, in this investigation we placed a pair of steel bias grids in front of the QCM to act as an ion filter, as shown in Fig. 13. The front

grid was biased to -30V to repel plasma electrons. The rear grid was biased to 300V and thereby acted to reject all ions, being that the thruster discharge voltage and maximum beam catcher bias were both 200V. We denote this pair of grids as the 'guard' and refer to the entire instrument as a 'guarded QCM.' When the guard was energized, all backstreaming ions were rejected and only backsputtered carbon particles would transport to the QCM, as illustrated in Fig. 13b. When the guard is turned off, both backstreaming ions and backsputtered carbon reach the QCM, as illustrated in Fig. 13a.

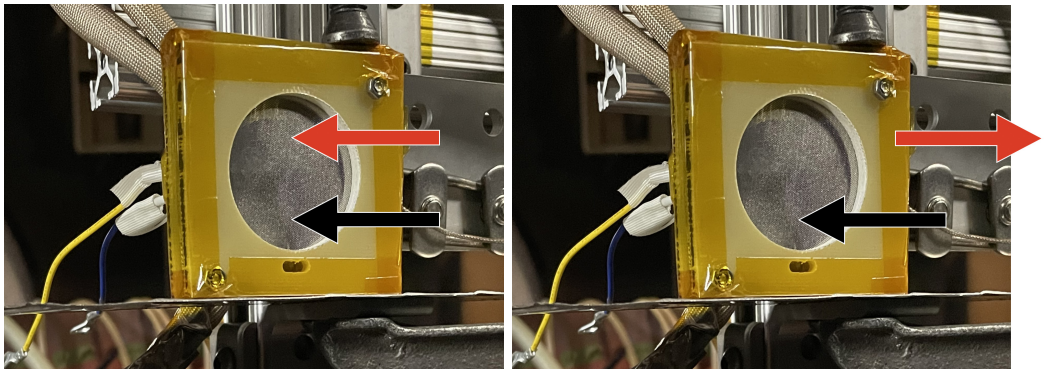

(a) Guard off, ion and carbon flux transit. (b) Guard on, ions rejected from QCM.

Figure 13: Photograph of guarded QCM and notional illustration of carbon and ion flux passing through the grids (black and red arrows, respectively). When no retarding bias is applied to the guard (13a) ion and carbon flux can both reach the QCM behind the grids. When a retarding bias is applied (13b), only carbon flux passes to the QCM.

The guard significantly attenuated the carbon backsputter flux that reached the surface of the QCM. We performed tests with the beam catcher grounded (i.e. no backstreaming ion flux) and measured carbon backsputter with and without the guard installed. With the guard installed, the backsputter rate was approximately 4% of the rate without the guard. We attribute this attenuation to carbon sputterants collecting on the grids. At these low signal levels the film thickness fluctuated over time, introducing uncertainty in the line fit used to calculate deposition rate. This is illustrated in Fig. 14. To quantify uncertainty, we again employed MCMC sampling to infer the fit parameters of the line. The deposition rate was taken to be the mean of the slope samples and a 95% confidence interval was obtained by computing the 2.5th and 97.5th percentile values of the samples. The line in Fig. 14 uses the most probable values for slope and y-intercept.

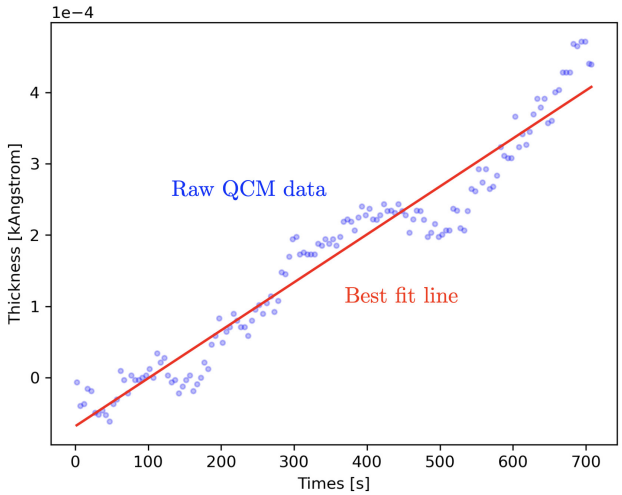

Figure 14: Raw QCM data and corresponding fit line. This data was taken at a plate bias of 125V and a cant angle of 20° and the line shown uses the mean (most probable) values for the slope and y-intercept.

D. Witness plates

While our investigation primarily focuses on the role of backstreaming ions on erosion rates, we also recognize that ions born in the near-field of the thruster may have sufficient energy when accelerating to the grounded QCM to induce erosion. This could be particularly problematic for high beam catcher biases which can cause a global increase in plasma potential with respect to facility ground.

With this in mind, to investigate the role of ambient (low-energy) ions–in addition to backstreaming ions–on backsputter deposition, we utilized an array of witness plates during Study 2. The array was mounted directly above the thruster and consisted of seven pairs of witness plates spaced 8.7 cm apart, as shown in Fig. 15. The left-most plate in Fig. 15 (labeled A) was aligned with thruster centerline. In each pair, one plate was acrylic and the other was aluminum and electrically connected to facility ground. In this manner, we could visually inspect the difference in film deposition between the insulative and grounded plates.

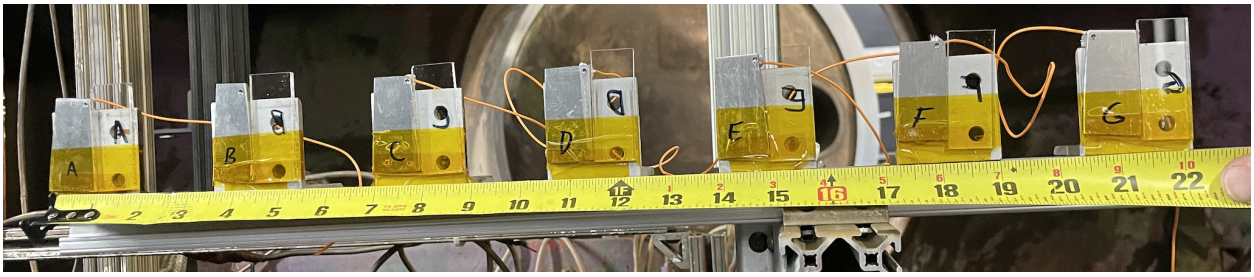

Figure 15: Photograph of the witness plate array employed in the second study to investigate the effect of grounded surfaces on carbon film buildup. The left-most witness plates were centered over thruster centerline.

VI. Results

In these studies we varied plate bias and cant angle and made measurements of the ions coming back from the beam catcher for a Hall thruster operating at a 2 kW (200V, 10A) discharge on argon propellant. In this passage, we first report the electrical characteristics of the beam catcher. We then overview the characteristics of the beam catcher plume and how they vary with cant angle and bias voltage. We then present how the backsputter varies with the beam catcher operating configuration. Finally, we show a comparison of witness plate measurements taken during the aforementioned tests.

A. Beam catcher electrical characteristics

To characterize the electrical performance of the beam catcher and its effect on the thruster plume, we conducted voltage sweeps of the beam catcher bias and measured the current necessary to maintain that bias, the cathode-to-ground (C2G) voltage, and the near-field plasma potential. Figure 16 shows these measurements as taken in Study 2. We omit measurements from Study 1 because we were unable to obtain reliable C2G measurements in that study; nevertheless, the plate I-V characteristic and plasma potential with respect to facility ground were in family with those from Study 2.

Figure 16a shows the plate current necessary to maintain a bias voltage across various cant angles. We note that these relationships trend similarly irrespective of cant angle. The physical implication of this result, as we discussed in Ref. 11, is that with increasing bias potential more electron current is drawn to the beam catcher. The role of the magnetic impedance is to restrict this current such that it does not exceed the total current available from the thruster. This ensures that the beam catcher can maintain a potential from the near field plasma.

To this point, we show in Figure 16b the variation in cathode to ground (C2G) voltage with bias voltage across various cant angles. Physically, we note that at low biases (<80 V), the C2G voltage remains relatively insensitive to bias but then increases more rapidly with higher values. This reflects the fact that the near-field plasma potential with respect to ground is adjusting to ensure that the total current to the beam catcher from ions to the chamber walls and electron current to the beam dump is balanced (Ref. 11). Figure 16d underscores this trend as we show the near-field plasma potential with respect to cathode as varying by less

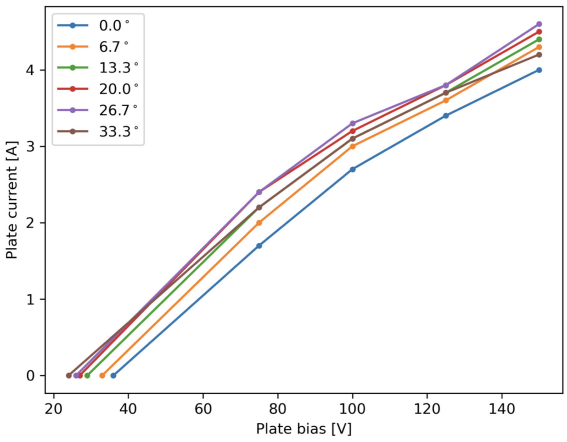

(a) Plate current draw vs. plate bias.

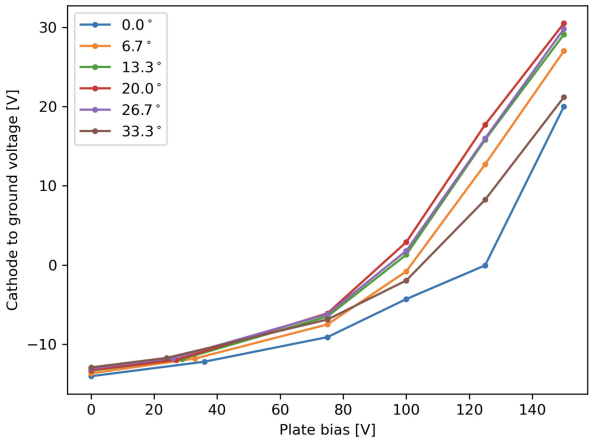

(b) C2G voltage vs. plate bias.

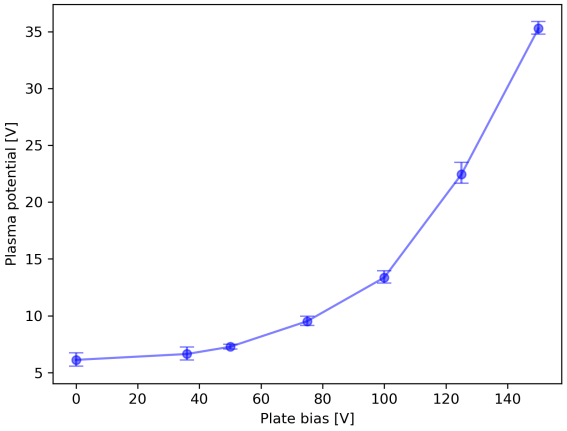

(c) Near field plasma potential w.r.t. facility ground.

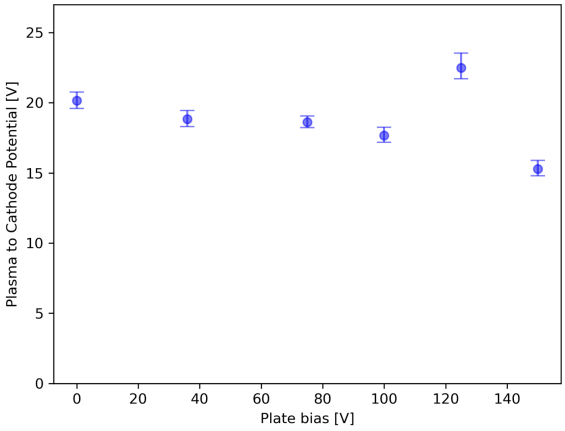

(d) Plasma potential w.r.t. cathode potential.

Figure 16: Beam catcher and plasma electrical characteristics from Study 2.

than 5V across 150V of applied bias. This is commensurate with our previous findings[11] and confirms the magnetic field is decoupling the bias and plume potentials.

To this point, Figure 16c shows the near-field plasma potential with respect to facility ground at 0° cant. This potential follows the C2G voltage and reflects the fact that the overall potential of the thruster with respect to ground is rising. Notably, the fact that cathode to ground and near field plasma potential with respect to ground increase at the same rate indicates that the potentials with respect to the thruster cathode are relatively insensitive to beam bias. We show this in Fig. 16d).

We note that the fact that near field plasma potential with respect to ground changes has potential bearing on our sputter measurements. Background ions born at these higher potentials may be accelerated into the grounded surfaces (such as the QCM) inducing erosion. We return to the significance of this latter result in Sec. VII.A.2.

B. Backstreaming ion characteristics

A primary objective of these studies was to identify whether canting the beam dump could mitigate the effects of backstreaming ion erosion at the QCM. This mitigation strategy relies on the hypothesis that a characteristic divergence angle of the backstreaming plume exists (see Fig. 3). To confirm this hypothesis, we used RPAs to measure spatial characteristics of the beam catcher plume.

1. *Radial RPA measurements at fixed beam catcher cant*

In Study 1, we took spatial measurements of the beam catcher plume by sweeping an outward-facing RPA through the thruster plume to measure the characteristics of radially-directed backstreaming ions. Figure 17a shows the most probable voltage (MPV) of backstreaming ions as a function of arm angle. This shows that at thruster centerline (which is located at 93°), radially-directed ions exhibit 80% of the applied bias energy. Between 15-25° of centerline, the MPV of radially directed ions from the forward tower falls to less than 50% of the peak bias energy beyond uncertainty.

Figure 17b shows the high energy ion current as a function of arm angle. To obtain the high energy ion current, we averaged the values of the raw RPA trace between biases of 40-60V (which we found to reliably fall between the low and high energy populations of ions) and took the standard deviation of these values to be the uncertainty. This average corresponds to the total current of all ions with more than approximately 50 eV of energy. As with the MPVs, Fig. 17b shows that within 15-25° of centerline, the current of radially directed ions from the forward tower falls by $> 50\%$, beyond uncertainty. It also shows that the MPV current is strongly correlated with distance, being that the forward tower exhibited approximately 60% higher currents than the rear tower.

Taken together, both charts in Fig. 17 show at least a 50% reduction in both MPV and radially directed current beyond 15-25° of thruster centerline, which implies the existence of a characteristic divergence angle in the range of 28.4-37.9°, given the geometry of the probe arm and the 27° cant angle of the plate in the Study 1 measurements.

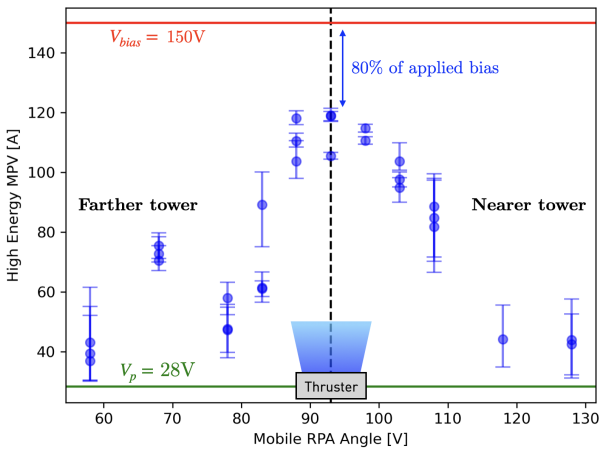

(a) MPV of radially directed ions with plate bias and near-field plasma potential marked.

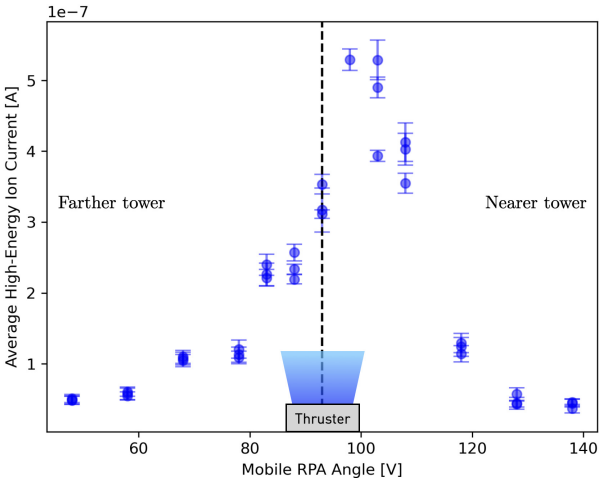

(b) Current corresponding to the MPV.

Figure 17: Measurements of radially-directed ions taken by the mobile RPA during Study 1 at 150V bias, 27° cant. Thruster centerline is located at 93°. Repeated measurements are plotted atop one another.

2. *Fixed RPA measurements at varied beam catcher angle*

Armed with the insight that the beam catcher has a characteristic divergence, we next examimed the impact of cant angle on the near-field properties at the thruster. To this end, we measured the MPV and current of high energy ions as a function of cant angle using the RPA fixed at the thruster plane. Figure 18a shows these measurements for Study 1 and Figure 18b shows these measurements for Study 2.

In both studies, the high energy ion current exhibits a maximum near 15°, and the ion current monotonically decreases with steeper cant angles. In Study 1, the measured ion current fell below the maximum value beyond uncertainty at 27° and observed a steep drop off above 34°, commensurate with the divergence angle implied by the radial sweep. In Study 2, the ion current fell below the maximum value beyond uncertainty at 23° but no steep drop off was observed. Given the placement of the probes in Study 2, we would expect a steep drop commensurate with the Study 1 result in the range 42-50°, which was beyond the range of motion of the beam catcher (this is discussed in Sec. VII.B). Physically, these results suggest that a divergence

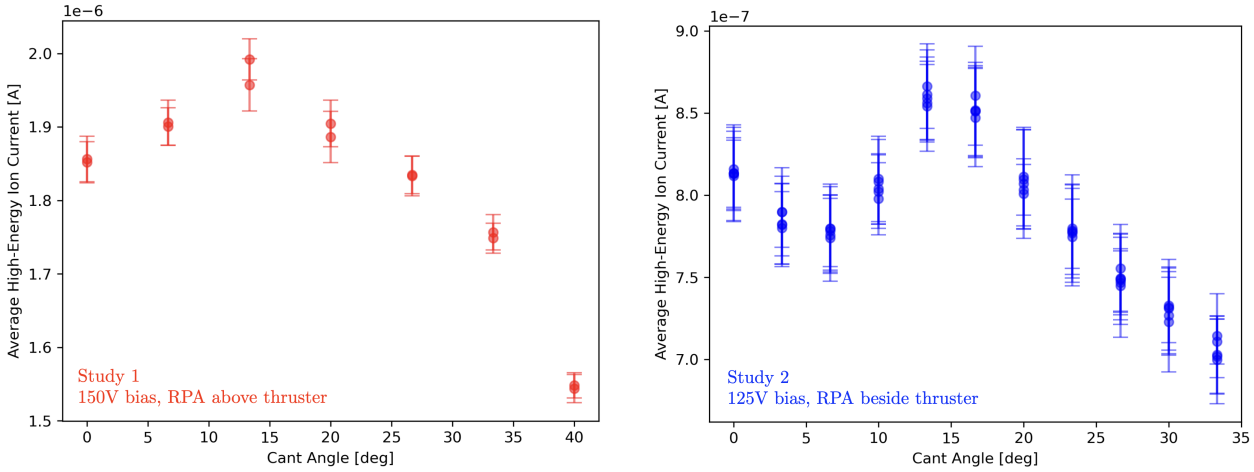

(a) Study 1 currents at 150V bias.

(b) Study 2 currents at 125V bias.

Figure 18: Current of the high energy ion population vs. plate angle at a fixed bias and probe location. Repeated measurements are plotted atop one another.

angle exists in the range of 34-40°. This is generally higher than–but still overlaps with–the range predicted by the radial energy measurements (28.4-37.9°)

C. Backsputter Measurements

To measure the effect of canting the beam catcher on minimizing backstreaming ion erosion and the effect of biasing the beam catcher on reducing carbon deposition, we performed guarded QCM measurements. With the guard off, these measurements capture the combined effect of ion erosion and carbon deposition; with the guard on, it measures only carbon deposition. In this section, we report QCM measurements made by parametrically varying both the plate bias and cant angle.

1. Varied Angle, Fixed Bias

Varying the beam catcher angle at a fixed bias provides insight into the effectiveness of canting the beam catcher at minimizing backstreaming ion erosion. Steeper cants would, in principle, reduce the flux of backstreaming ions to the thruster and therefore reduce the magnitude of negative backsputter rates (see Fig. 18). Figure 19 shows the effect of varying cant angle on QCM measurements with and without the guard on. In Figure 19a, the ion erosion rate exhibits a reduction with cant angle up to 27-34°. In Figure 19b, the ion erosion rate generally decreases with cant angle. Given the placement of probes in Study 2, we would expect to observe a minimum ion erosion rate commensurate with the Study 1 minimum in the range 35-42°, which is beyond the range of motion of the beam catcher.

Physically, these results suggest that a divergence angle exists in the range of 27-34°. This is lower than the range predicted by RPA current measurements (34-40°) but agrees with the range predicted by RPA energy measurements (28.4-37.9°). It is also significant to note that in neither study the erosion rate reached zero. This could suggest the presence of additional erosion effects. We discuss the possibility of erosion from background plasma ions in Sec. VII.A.2.

2. Varied Bias, Fixed Angle

Figure 20 shows the result of varying bias at a fixed angle of 27° during Study 1. We selected this angle for Study 1 because it exhibited the minimum magnitude of backstreaming ion erosion per Fig. 19a. Figure 21 shows the result of varying bias at a fixed angle of 0° during Study 2. We selected no cant for Study 2 in order to maximize the signal of both backsputter and ion erosion, being that deposition rates were substantially attenuated by the guard grids.

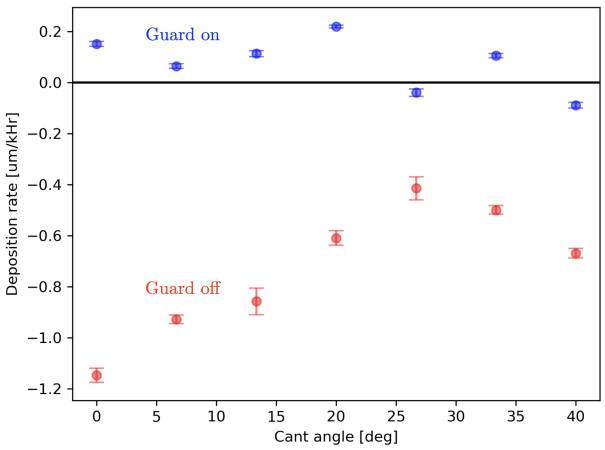

(a) Study 1, at 150V plate bias.

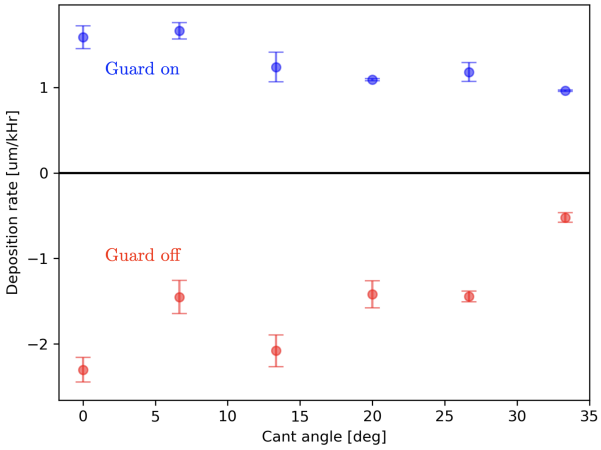

(b) Study 2, at 125V plate bias.

Figure 19: Guarded QCM measurements for both studies at fixed plate biases.

Due to constraints in recording time, in these measurements we chose to take data at higher angular resolution with the guard on and measured only three angles each with the guard off. It is notable that the deposition rates (measured with the guard on) in both studies exhibited two behaviors: decreasing up to 75V of bias and increasing beyond 75V of bias. Decreasing deposition up to 75V is expected behaviorand we observe deposition reductions of 45.4% and 9.5% between the floating potential and 75V in Studies 1 and 2, respectively.

Increasing deposition beyond 75V is unexpected behavior given that with the grid on, we have eliminated the impact of backstreaming ions. The only effect that should remain is the rate of actual backsputter from the beam dump, which should decrease with beam catcher bias. As a possible explanation of this trend, we consider the possibility of sputtering of the grids themselves. Backstreaming ions accelerate through approximately 75-80% of the bias voltage (Fig. 17a), hence backstreaming ions at 75V plate bias possess >56-60 eV of energy. This is sufficient to sputter iron from the stainless steel guard grids to the QCM, thus leading to the effective increase in deposition. We expand on this possibility in detail in Sec. VII.C.1.

To obtain a rough estimate for the net reduction in backsputter at 150V of bias (which is obscured by guard sputtering), we scaled our predicted sputter yield curve for carbon (which discussed in Sec. VII.C.1) to match the 45.4% reduction observed at 75V of applied bias. Using this scaled curve we estimate the backsputter reduction attained at 150V to be 73.8%.

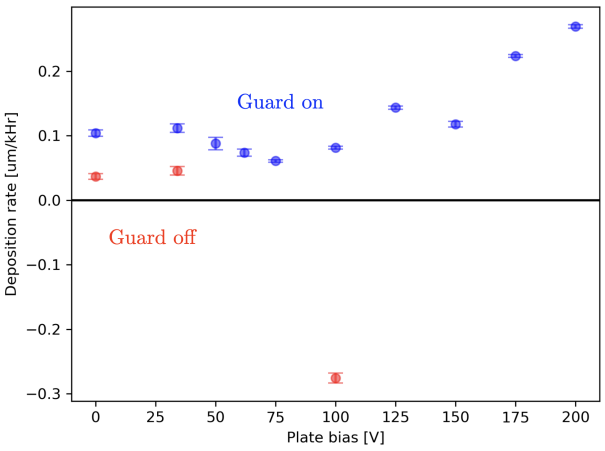

(a) Study 1, all measurements.

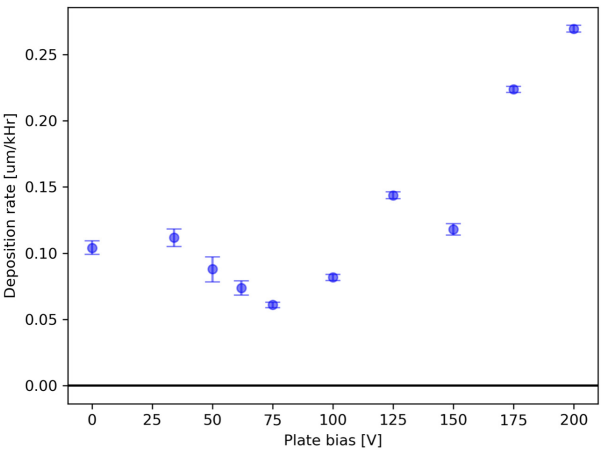

(b) Study 1, only guard on.

Figure 20: Guarded QCM measurements for Study 1 with a fixed cant angle of 27°.

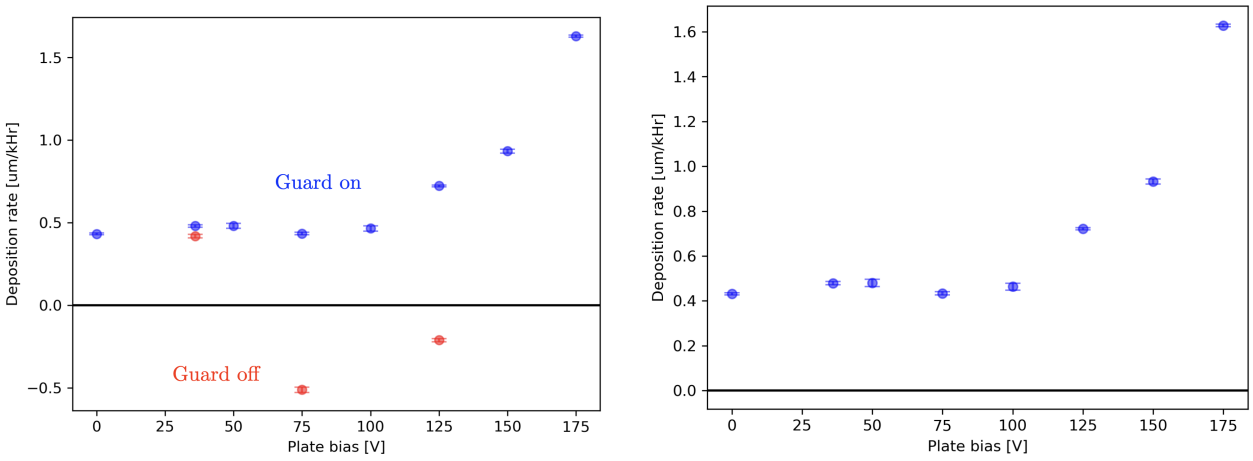

(a) Study 2, all measurements.

(b) Study 2, only guard on.

Figure 21: Guarded QCM measurements for Study 2 with a fixed cant angle of 0°.

D. Witness Plates

In both sets of QCM measurements taken at a fixed bias with varied angle (Fig. 19) it can be seen that the negative backsputter rate improves with cant angle but does not reach zero. Furthermore, in Study 1 the QCM measurements taken at low bias voltages (see Fig. 20a; 0V, 34V) with the guard off exhibited lower values than with the guard on, even in the absence of energetic backstreaming ions. We hypothesized that both of these phenomena could be caused by the background plasma potential being sufficiently high for ions to be accelerated into grounded surfaces (such as the QCM) with sufficient energy to cause sputtering. To test this hypothesis, in Study 2 we installed the array of witness plate pairs described in Sec. V. We employed the plate array for approximately 16 hours of active beam catcher testing followed by 8 hours of additional thruster testing with the beam catcher grounded.

Before and after photos of the witness plate array are shown in Figure 22. Close-up photos of each witness plate pair are available in Appendix E. By inspection, a gray carbon film was visible building up on insulative surfaces (kapton tape, acrylic) but not on grounded surfaces. In addition, carbon film deposition on the acrylic plates exhibited a gradient with distance from the thruster, showing that carbon deposition falls substantially with distance from thruster centerline.

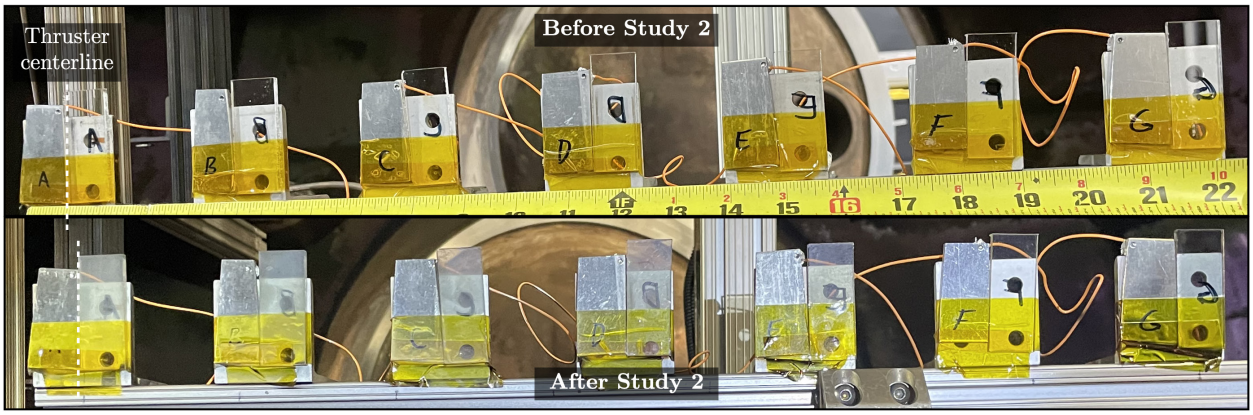

Figure 22: Photos of the witness plate array before and after Study 2. By inspection, gray film builds up on electrically insulating surfaces but not on grounded surfaces.

These findings suggest that the location of the QCM and erosion from background plasma ions may be substantial sources of uncertainty when attempting to estimate the backsputter rate at a thruster. It is already known that the deposition rate at a QCM varies spatially,[18] hence the gradient in distance from the

thruster is not unexpected. The finding that background ions erode material from grounded surfaces has not previously been reported. A possible mitigation would be to locate the QCM farther from the thruster (where plasma density is lower), but this must be balanced with the fact that carbon deposition also decreases with distance. The ion erosion effect must therefore be characterized in order to make accurate estimates of carbon deposition on critical thruster surfaces.

In this section we have reported the results of our characterization studies. We showed that the beam catcher can support large retarding potentials while minimally affecting the near-field plasma-to-cathode potential. We also showed that large biases cause the near-field plasma potential to rise with respect to facility ground. By measuring the properties of ions returning from the beam catcher, we confirmed the existence of a characteristic divergence angle for backstreaming ions and place that divergence angle in the range of 27-34°. We found that negative backsputter rates can be improved–but not entirely eliminated–by canting the beam catcher. This implies that background plasma ions may be sufficiently energetic to erode material from the QCM, a possibility corroborated by our installing witness plates and finding that carbon films did not build up on grounded surfaces. Now that we have presented the results, we examine key implications in the following section.

VII. Discussion

In this section, we begin by discussing sources of uncertainty in the results and then discuss how the results address the questions of how to reduce backstreaming and the effectiveness at reducing carbon backsputter. We conclude this section by discussing strategies for future probing techniques to reduce measurement uncertainty.

A. Sources of uncertainty in results

Throughout these studies, we observed variations in QCM measurements across timescales of both minutes and hours that introduced uncertainty to our measurements of deposition rate. Here, we show evidence of these uncertainties and discuss emission of adsorbed volatiles and erosion from background plasma ions as two potential causes.

1. Variation of QCM measurements at short and long time scales

To obtain each deposition rate estimate, we measured the QCM film thickness at a constant thruster/beam catcher operating condition over a 15-20 minute recording window. We expect deposition to be a linear process, so we obtain a rate by fitting a line to the data. Figure 23 shows two raw QCM traces at 0V bias, 0° cant angle, one with the guard installed and one without. Without the guard installed (Fig. 23a), the deposition is highly linear by inspection. With the guard installed (Fig. 23b), the deposition varies over the 'short' timescale of minutes, introducing uncertainty to the line fit. The consequence of these short timescale fluctuations is an increase the uncertainty in each individual rate measurement. Although the cause of these fluctuations is unknown, it appears that these fluctuations are negligible when the guard is removed.

We also observed drift effects over the 'long' time scale of hours. This is illustrated in Fig. 24, which shows the results of repeated measurements taken during Study 2 at a 125V plate bias. Figure 24a shows measurements made with the beam catcher grounded at 0° cant (i.e. no backstreaming ions present). It is notable that the guard on measurements *after* the first four hours of thruster operation are equal within uncertainty. We hypothesize that during the first few hours of exposure to the ion beam, the beam catcher releases adsorbed volatiles or loses an easily sputtered surface oxide layer and particles from either of these sources deposit on the QCM at enhanced rates. The effect of this volatile emission process is an artificial enhancement in deposition rates during the first hours of testing. Figure 24a shows that four hours is an upper bound on the time for this effect to settle. All Study 1 data we report were collected after four hours of thruster operation. In Study 2, the varied angle, fixed bias data (Fig. 19b) up to 20° were collected before 4 hours of operation. All other data in Study 2 were collected after 4 hours of operation. This raises the possibility that the guard on measurements in Fig. 19b are artificially high.

An additional long time scale phenomena we observed was an attenuation in the negative backsputter rate signal. Figure 24b shows measurements made with the beam catcher at 125V bias at a variety of

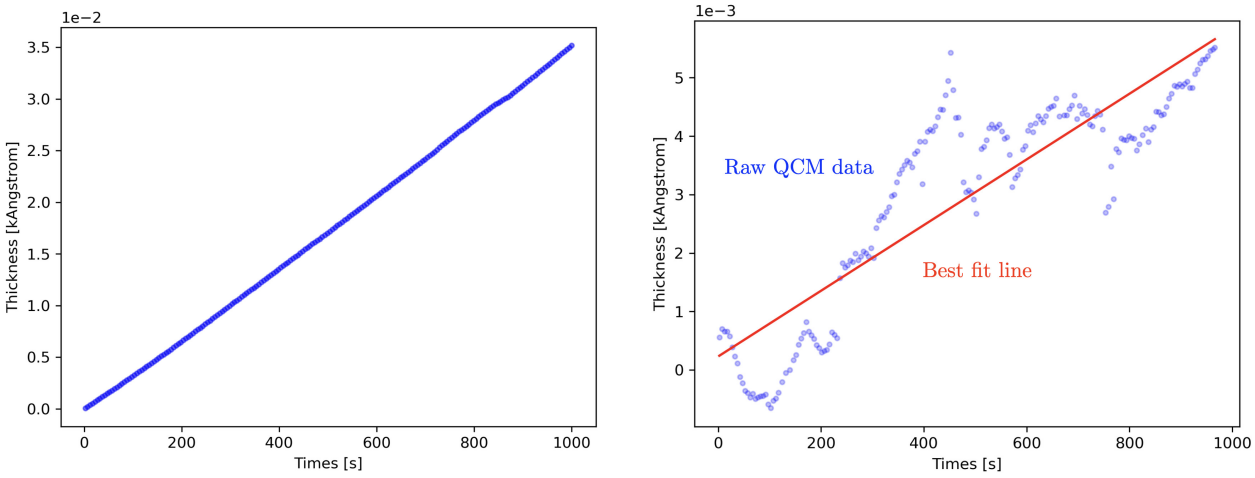

(a) Raw QCM measurement following Study 2 at 0V bias, 0° cant with guard removed.

(b) Raw QCM measurement from the start of Study 2 at 0V bias, 0° cant with the guard on.

Figure 23: Raw QCM measurements with and without a guard installed.

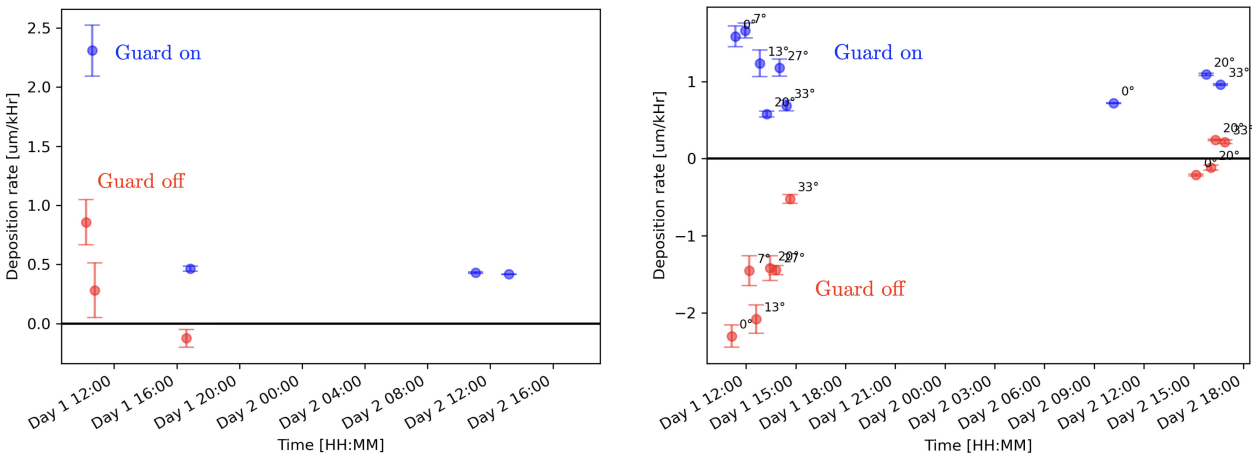

(a) (b)

Figure 24: Repeated QCM measurements from Study 2 with the beam catcher (a) grounded at 0° cant angle and (b) biased to 125V (at all angles).

cant angles. By inspection, the magnitude of the backsputter rates observed with the guard off are tightly clustered near zero on Day 2 as compared to the corresponding rates observed on Day 1.

2. Erosion induced by background plasma ions

Throughout these studies we observed phenomena that imply that the background plasma may have an erosive effect on grounded surfaces. Qualitatively, we observed this in the witness plate study, in which the grounded plates which did not appear to accumulate a carbon film (see Fig. 22), even as immediately adjacent acrylic witness plates did. We also observed this qualitatively in the varied angle (see Fig. 19), fixed bias studies in which negative deposition rates approached–but never reached–zero, even at steep cant angles.

Quantitatively, we observed this effect in QCM measurements from both studies. Figure 25a shows a result from Study 1 in which the deposition rate with the guard on and off differs when the beam catcher is grounded (0V) and electrically floating at 34V. The difference in deposition rates at these potentials are

0.0672 um/kHr and 0.0662 um/kHr, respectively, being identical within uncertainty. This observation is corroborated by Study 2, as shown in Fig. 25b. Here, the difference between guard on and off is 0.0619 um/kHr, falling within 10% of the measured deltas from Study 1. We theorize that the disparities in deposition rates between guard conditions are caused by the guard bias preventing background, low-energy ions from reaching the QCM. At these low beam catcher biases, only background ions could plausibly be a source of sputtering.

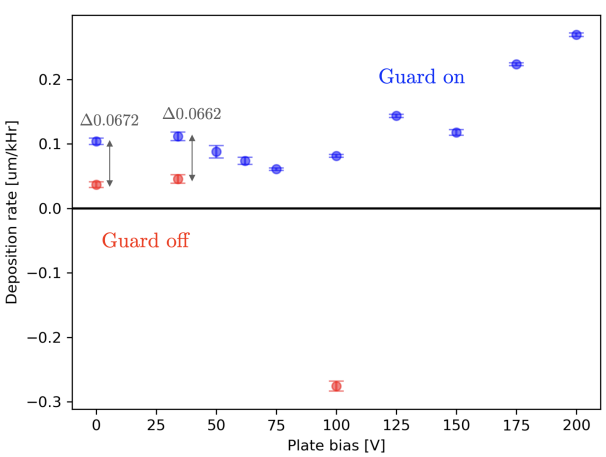

(a) Study 1, 27° cant (Fig. 20a, annotated).

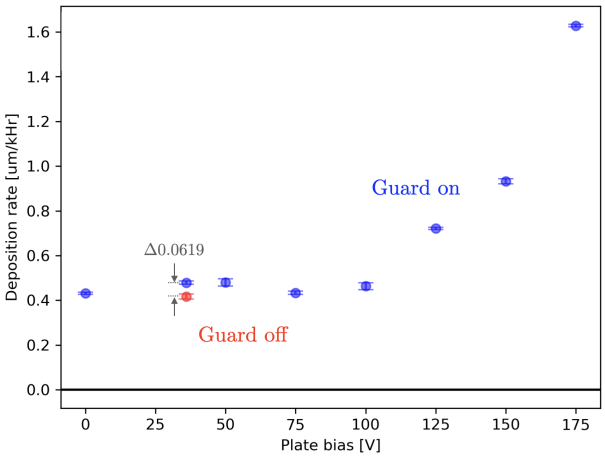

(b) Study 2, 0° cant (Fig. 21a, annotated)

Figure 25: Guarded QCM measurements with low-voltage measurement differences annotated.

To this point, Figure 16c, shows that the near-field plasma potential at low plate biases generally falls within 5-10V of facility ground. To examine whether these ions are capable of inducing erosion, we turn to the sputter threshold energy for graphite. Yim[14] uses xenon data to predict a sputter threshold energy of 21V for xenon-graphite bombardment. Using argon-carbon data, we predict (using analysis described in Sec. VII.1) a sputter threshold energy of 21.6V (the analysis of this is described later in this section). Although the near-field plasma potential falls below either threshold energy, both Yim and we obtain confidence intervals that place the sputter threshold as low as 5.3-6V, which is within the plasma potential observed at low plate biases. This raises the possibility that the background near-field plasma may introduce uncertainty to QCM measurements by eroding material from the QCM even at low plasma potentials. We expect that the severity of this background erosion will rise with applied plate bias because higher plate biases increase both background plasma density and the plasma potential relative to ground (i.e. relative to the QCM surface).

Taken together, we see that poorly characterized processes including background ion erosion and volatile emission introduce measurement variations over both short and long time scales. This has the effect of increasing the uncertainty in estimating individual deposition rates and in introducing drifts in measured rates over hours of testing. Although the exact causes of these fluctuations are unknown, we have identified potential causes mitigations. We note that signal strength enhancement may be achieved with probe techniques that do not require grids to be placed over the QCM. This is discussed in Sec. VII.D

B. Canting as a mitigation for ion backstreaming

To evaluate whether canting the beam catcher can be used as a mitigation for ion backstreaming, we measured the variation of three quantities with cant angle at a fixed plate bias:

1. The energy of backstreaming ions. Physically, this energy represents the ability of a single bombarding ion to erode material at the thruster (as illustrated by the sputter yield curve in Fig. 1).

2. The current of backstreaming ions. Physically, this current represents the number of ions arriving at the thruster per unit time, and thereby the number of ions available to cause erosion.

3. The erosion rate at the thruster. This is the macroscopic quantity we seek to mitigate by canting the beam dump.

Below, we discuss how the above measurements address the effectiveness of canting as a backstreaming ion mitigation. Throughout this section we use 'backstreaming ions' to refer specifically to the high-energy population of ions launched back at the thruster by the beam catcher.

1. *QCM erosion rates*

The guarded QCM provides a direct measurement of the macroscopic impact of backstreaming ion erosion. Figure 19 shows the effect that varying the beam catcher cant angle has on the net carbon deposition/ion erosion rate measured by the QCM. With the guard off (allowing both ion and carbon flux to reach the QCM), Study 1 exhibited a 64.0% reduction in the magnitude of the (negative) deposition rate over the range 0° to 27°. We saw a similar trend in Study 2, which exhibited a 77.4% reduction in the magnitude of the (negative) deposition rate over the range 0° to 33°. However, Study 2 did not exhibit a minimum as in Study 1. An explanation for this may again be found in the difference in probe placement between studies; a minimum observed at 27° in Study 1 would manifest at 35.26° in Study 2, which was beyond the range of motion for the towers.

It is significant to note that although varying cant angle reduced the magnitude of ion erosion in both studies, it did not appear to drive ion erosion to zero in either. As previously discussed, one interpretation of this result is that steep cant angles do eliminate backstreaming ion erosion and the residual erosion is due to background plasma ions. Figure 25, shows higher deposition rates with the guard on than with the guard off at low plate biases; this feature evidences erosion from the background plasma, which would be the only source of ions at low plate biases (i.e. the beam catcher is not backstreaming ions when the bias plate is at/near ground). We found that at these low plate biases, the background plasma potential w.r.t. ground measured 5-10V (see Fig. 16c) and expect erosion from background ions to increase with applied beam catcher bias due to the beam catcher's raising the plasma potential. Figure 16c) shows that the plasma potential increases to 23V at 125V of plate bias. This increases the potential difference that background ions are accelerated through before striking the QCM crystal (which is necessarily grounded) and therefore the sputter yield from the crystal. As a result, further analysis is required to characterize this level of ambient erosion and its variation with plasma potential. We also note that a potential mitigation for the plasma potential rising with plate bias is to apply a stronger magnetic field.[11]

C. Effectiveness at Reducing Carbon Backsputter

In this section, we begin by anticipating the level of attainable backsputter reduction and then discuss the two distinct behaviors seen in the QCM data. We then discuss additional observations that imply background plasma effects that may not have been previously accounted for.

To estimate the maximum level of attainable backsputter reduction, we turned again to the *Sputterer* modeling tool. Following the conclusion of testing, we input the true configuration of the beam catcher array into *Sputterer* and evaluated backsputter levels as a function of cant angle with the beam catcher bias plates as 1) a surface that sputters like carbon and 2) a surface that is perfectly non-sputtering. A perfectly non-sputtering surface corresponds to a bias voltage that perfectly decelerates all incoming ions (e.g. 200V in this study). Figure 26 shows the results of these simulations.

In Study 1 we varied bias voltage at a fixed cant of 27°. Simulations predict a maximum backsputter reduction of 78%. In Study 2, we made QCM measurements at 0°, yielding a theoretical reduction of 88%. We expect higher deposition rates in experiment than predicted by simulation because 1) the beam catcher is not truly non-sputtering and 2) *Sputterer* fails to model the steel boundaries of the facility, which will also contribute to backsputter. Thus, we take the simulation results to represent a theoretical maximum reduction.

Measurements of the rate of QCM deposition as a function of bias voltage for Study 1 (fixed 27° cant) are shown in Fig. 20. In this configuration, *Sputterer* predicts a theoretical maximum reduction of 78%. At 75V, we measured a reduction of 45.4%. To compare our actual result to the simulated backsputter reduction, we interpolate the simulation result in the following manner:

- We assume beam ions to leave the thruster at 180 eV.
- Using the sputter yield curves discussed below (Sec. VII.C.1), we find a sputter yield reduction of 62.5% for 180 eV ions decelerated through a 75V potential.

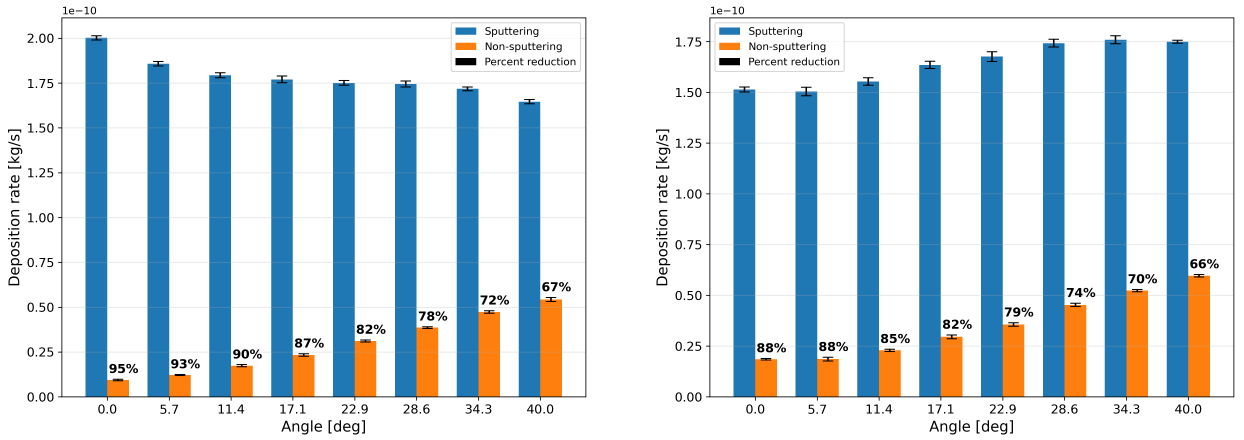

(a) (b)

Figure 26: *Sputterer* simulation results reflective of actual beam catcher configuration in (a) Study 1 and (b) Study 2. The *reduction* in backsputter between the beam catcher bias plates being modeled as sputtering or perfectly non-sputtering is reported as a percentage.

- We scale the perfectly non-sputtering reduction of 78% by 62.5% to obtain a prediction of 48.7% reduction at 75V.

Our observed 45.4% reduction closely aligns with the simulated prediction of 48.7%. Figure 27a shows a graphical comparison of the various simulation results and the actual measurement.

Measurements of deposition for Study 2 (fixed 0° cant) are shown in Fig. 21. In this configuration, *Sputterer* predicts a maximum reduction of 87.8% and at 75V, we measured a reduction of 9.5%. Using the same interpolation scheme, we predict a reduction of 54.9% at 75V. These reductions are compared graphically in Fig. 27b. Although the reason for the beam catcher's poor performance at these conditions is not immediately apparent, potential causes include all previously mentioned sources of uncertainty in QCM measurements.

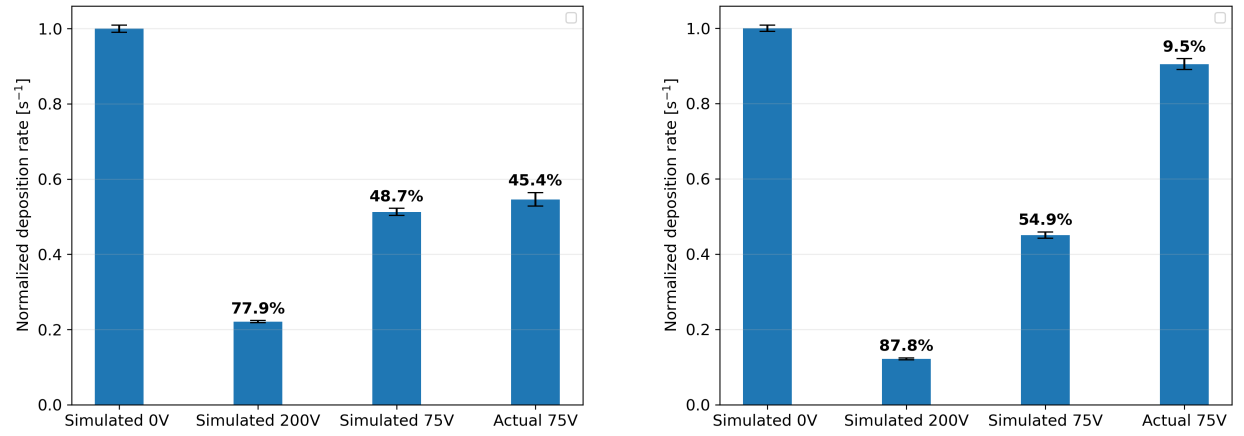

(a) (b)

Figure 27: Comparison of simulated and observed reductions in backsputter for (a) Study 1 and (b) Study 2. The *reduction* in deposition is reported as a percentage.

To estimate the level of backsputter reduction attained in Study 1 at 150V of bias (which could not be measured directly due to suspected guard grid sputtering), we scaled a predicted carbon sputter yield curve to match the 45.4% reduction observed at 75V of bias (assuming 180 eV beam ions). Our method of

obtaining the initial carbon sputter yield curve is detailed below in Sec. VII.C.1. Using the scaled curve, we computed the backsputter reduction at 150V of bias (30 eV bombarding ions) to be 73.8%. Although this is a speculative estimate, we note that it is commensurate with the theoretical backsputter minimum for Study 1 of 78% (Fig. 26a).

Taken together, these data are evidence that backsputter rates are reduced by increasing plate bias up to 75V of bias. Notably, Study 1 exhibits backsputter reduction rates commensurate with theoretical minimums predicted by computational modeling. Further investigation of noise processes must be undertaken to interpret the results of Study 2.

1. *Deposition Increase at High Biases*

Beyond 75V, the deposition rate in both studies increases with applied bias. This is an unexpected result given that higher plate biases should have the effect of reducing sputter yield at the beam dump. Our explanation is that backstreaming ions are sputtering material off of the QCM guard grids. To support this conclusion, we estimated sputter yield curves for argon ions incident on carbon and iron using a technique similar to Yim[14] in performing Bayesian parameter fitting using the Markov Chain Monte Carlo (MCMC) algorithm. Specifically, we use MCMC to infer fit parameters for the Eckstein model[14,16] using empirical data reported by Behrisch and Eckstein[16] for argon ions incident on carbon and iron. This enables us to compare the threshold energy and relative steepness of the sputter yield curves. Details on how we performed this inference are given in Appendix D. We note that the confidence intervals over the fit parameters were large and so these results *should not be relied upon for detailed analysis*; nevertheless, the relative comparisons of threshold energy and curve steepness inform the situation encountered in this study.

Figure 28 shows the sputter yield curves we obtained. We note two key features: first, the sputter threshold energy, E_{th}, for iron is higher than carbon. Physically, this represents the minimum energy a bombarding ion must have to cause sputtering. We found the most probable E_{th} for carbon to be 21.6 eV and the most probable E_{th} for iron to be 37.3 eV. The second key feature is that the iron curve exhibits greater steepness than the carbon curve, enabling it to dominate the sputter environment at ion energies >39 eV. We observed backstreaming ions to possess approximately 75-80% of the bias plate energy. Thus, at a plate bias of 75V, backstreaming ions possess approximately 56 eV of energy. Figure 28 shows that at 56 eV of energy, the sputtering of iron is an order of magnitude higher than the sputtering of carbon.

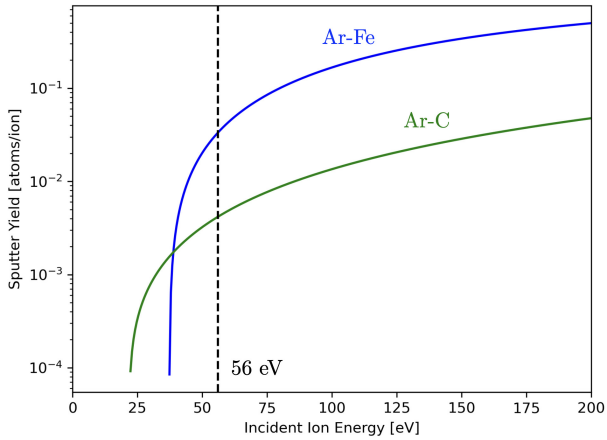

Figure 28: Eckstein model fits to available data for argon bombardment of carbon and iron. Backstreaming ion energy is approximately 56 eV at 75V of applied bias.

For this reason, we attribute the increasing deposition rates above 75V to backstreaming ions sputtering material off the steel grids in front of the QCM. Further evidence for this hypothesis is found in the QCM measurements from Study 2, shown with annotations in Fig. 29. The difference between measurements with the guard on and off is 0.9460 um/kHr at 75V and 0.9331 um/kHr at 125V. This observation is consistent with a process that increases deposition at the QCM surface (i.e. iron grid sputtering) in the presence of an erosion level that slightly increases (i.e. carbon sputtering off the surface of the QCM at low rates compared to iron buildup).

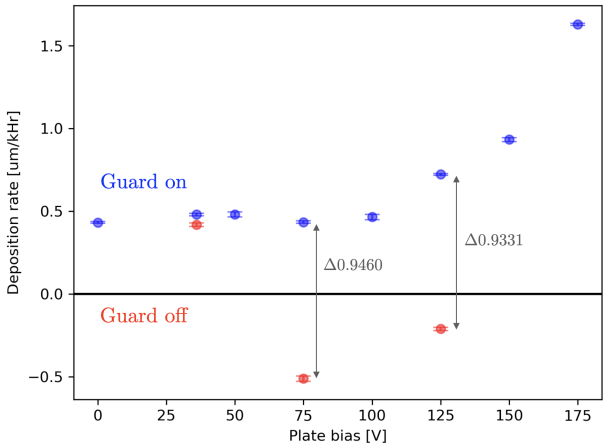

Figure 29: Study 2, 0° cant (Fig. 21a) with annotations for the differences between guard on and guard off measurements.

D. Next generation beam catcher testing

Throughout this study, we have seen that the cusped-field beam catcher demonstrates promise as a device for reducing backsputter in ground test environments. However, limitations in probing and challenges in scaling (both in physical size and for high power thrusters) need to be addressed before the beam catcher can be deployed in contemporary test facilities.

First, we address the limitation of the guarded QCM. This probe allows us to deconvolve the effects of backstreaming ions and carbon deposition but introduces the problems of signal attenuation and grid sputtering. One method for measuring deposition without grids would be to apply a magnetic field parallel to the QCM crystal to deflect incoming ions. An example can be seen in the magnetically filtered Faraday probe tested by Rovey et al.[19] A very strong magnetic field is required to deflect backstreaming ions with energies exceeding 150 eV, but permanent magnets such as the ones used to create the cusped field in this beam catcher are capable of producing such fields over the length scales needed to filter a QCM. This magnetic filter would strengthen the QCM signal and eliminate guard sputtering as a source of error.

Once an improved backsputter measurement technique has been developed, we can turn to challenge of physically scaling the beam catcher. We have previously seen that the solenoid beam catcher does not scale favorably due to the solenoids' large power requirements,[11] weight, and sputtering target area. The cusped field design addresses these limitations and can be scaled easily in either planar axis by increasing the length of magnetic rails or by adding more rails in parallel. Alternatively, many small beam catcher panels could be assembled and tiled together. To mitigate backstreaming ion erosion, we have shown that a staggered wedge shape attenuates erosion at the thruster plane and that the beam catcher exhibits a characteristic divergence angle of 34○ at most severe. Given a downstream distance from the thruster (defined by the test facility), the installation cant angle needed to establish an ion-free window at the thruster can be easily determined.

When considering thruster power scaling, a primary constraint for any permanent magnet beam catcher is temperature. Our neodymium magnets have a maximum operating temperature of 80°, which we stayed comfortably below by establishing a vacuum gap between the bias plate and magnetic rails to provide thermal isolation (over four hours of continuous exposure to a 1 kW discharge, the magnets closest to the center of the plume rose from -4°C to 10°C). For a thruster discharge in the tens or hundreds of kilowatts, additional thermal mitigations will likely be needed. One mitigation strategy would be to insert multi-layer insulation between the magnets and bias plate. Another would be to water cool the graphite plate (which has the added benefit of reducing heat flux to all surfaces in the facility, such as upstream cryopumps).

Another concern for thruster power scaling is the beam catcher power draw needed to maintain a retarding bias. If either the thruster current or power are increased (which would create a higher current density at the bias plate or necessitate a higher bias voltage, respectively), the requisite beam catcher power draw will rise. We have previously reported a model for the current draw needed to maintain a fixed bias voltage[11] which shows that enhancing the magnetic field strength attenuates the current draw needed to maintain a fixed bias voltage. Thus, when scaling the beam catcher for higher power thrusters it will become advantageous

to establish the strongest magnetic field possible.

VIII. Conclusion

Backsputter of facility material poses a major challenge to testing contemporary electric propulsion thrusters by obscuring measurements of thruster lifetime and enhancing the risk of arcing. The magnetically-assisted, electrostatically-retarding 'beam catcher' has previously shown promise as a tool to mitigate backsputter, but deposition measurements were confounded by the presence of high energy ions backstreaming from the beam catcher. In this work, we evaluated the effectiveness of canting the beam catcher as a mitigation for backstreaming ions and measured carbon deposition rates without the effect of ion erosion by means of an electrostatically filtered QCM.

We built two cusped magnetic field beam catcher panels each measuring 1.2×0.66 m. To investigate whether backstreaming ions could be directed away from the thruster by the beam catcher's electric field, we installed these panels on rotating towers and varied the cant angle in situ. We measured the properties of backstreaming ions using a suite of probes mounted near the thruster. To evaluate the effectiveness of bias voltage on reducing backsputter, we employed an electrostatically filtered QCM to measure deposition without the effect of backstreaming ions. We performed two parametric studies of this actuated beam catcher in the plume of a 2 kW argon Hall thruster.

In both of our studies, we observed negative erosion rates commensurate with previous studies, then proceeded to show that the magnitude of this rate (which is driven by ion erosion) shrinks with cant angle. In Study 1, we reduced the negative deposition rate by 64% at a 27° cant; in Study 2, we reduced negative deposition by 77% at a 33° cant. This confirmed that canting the beam dump can serve as a mitigation for backstreaming ion erosion. However, neither study was able to drive the negative deposition rate to zero. While this could be caused by a persistent backstreaming ion population, we obtained qualitative and quantitative evidence that background ions possess sufficient energy to induce a baseline level of erosion on grounded surfaces, such as the body of the QCM. A limitation of this study is that we were unable to characterize this level of background erosion and therefore cannot conclude whether canting the beam dump completely mitigates backstreaming ion erosion.

In both studies we were able to resolve positive deposition rates at high biases using the filtered QCM (a result not attainable in previous work). In Study 1, we measured a 45.4% reduction in deposition up to 75V of bias, a level commensurate with a theoretical maximum of 48.5% predicted by computational modeling. In Study 2, we observed a 9.5% reduction in deposition up to 75V of bias. In both studies, we observed a rise in deposition rate above 75V of plate bias. We attribute this effect to 75V being a threshold bias above which backstreaming ions sputter material off of the steel grids used in the QCM's electrostatic filter. We support this conjecture with sputter yield curve modeling of iron and carbon bombardment by argon.

Ultimately, this work demonstrates that a magnetically assisted, electrostatically retarding beam dump is capable of reducing backsputter rates up to 75V and that canting the bias plates of this beam catcher attenuates the effect of backstreaming ions on the thruster. We also showed that background plasma ions may have an erosive effect on grounded surfaces even at low plasma potentials. Limitations of this study are that we were unable to characterize this background level of erosion or measure backsputter rates above 75V on account of the design of the filtered QCM. Nevertheless, we propose avenues for future probing and options for addressing physical and thruster power scaling challenges for more advanced beam catchers. This work thereby demonstrates that the beam catcher is a potentially effective and scalable path for enhancing ground testing of next-generation propulsion systems.

Acknowledgements

This work was partially supported by NASA through the Joint Advanced Propulsion Institute, a NASA Space Technology Research Institute, grant number 80NSSC21K1118; by DARPA through the Thruster Advancements for Low-altitude Operations in Space (TALOS) research program; and by the National Science Foundation Graduate Research Fellowship Program. The authors would like to thank Seth Thompson for helpful advice surrounding sputter yield curve estimation and Ian Eykamp for discussions that led to the guarded QCM concept.

Appendix

A. Sputterer Simulations

To identify the placement of the beam catcher in the facility that would most significantly reduce backsputter, we performed carbon deposition simulations using the *Sputterer* code developed by Marks.[15] In these simulations, we employed a representative CAD model of the beam catcher deflector panels and support structure. We modeled the bias plates as perfectly non-sputtering surfaces and the support structure as graphite (being that we wrapped all support structures in grafoil or grafelt). We did not model the metallic walls of the test facility in the chamber but did include a passive beam dump representative of the facility geometry downstream of the beam catcher.

The output of a *Sputterer* simulation is the number of carbon particles collected by a target surface as a function of time. We designated two square collection surfaces at the thruster exit plane, one in the center of the ion beam (representing a thruster) and one to the left of the thruster (representing our quartz crystal microbalance). These features are visible in Fig. 7a. Each run simulated 100 milliseconds of thruster operation with a time step of 0.3 milliseconds and a macroparticle size of 5×10^{10}. Every 10 time steps, we logged the total number of particles collected on on each collection surface. We chose these simulation parameters by performing a convergence study for deposition rate over the four aforementioned parameters while aiming to minimize simulation runtime. To obtain a deposition rate, we fit a line to the output data.

There were three geometric parameters of interest to us in these studies: the distance from the thruster (range), the gap between the towers (width), and the cant angle (angle).

The **range** was the key parameter of interest because of the balance of two effects. At short range, the support structure can become a dominant source of backsputter and steep cant angles may be needed to deflect backstreaming ions, thereby reducing the plate's cross sectional area. At long range, less of the thruster beam is subtended, thereby enhancing backsputter from the passive facility. Thus, we sought to identify an optimal range for the beam catcher that balances these effects.

The presence of a gap **width** between the beam catcher towers allows some of the ion beam to pass through. This reduces backsputter by shifting the support structure into lower-density regions of the beam. However, the gap also enables a portion of the beam (which is not decelerated) to sputter surfaces downstream of the beam catcher. We theorized that a substantial fraction of these sputterants might adhere to the back of the beam catcher. Thus, we sought to identify whether an optimal gap width existed to maximize the effects of minimizing support structure backsputter and shadow shielding carbon flux from behind the beam catcher.

The cant **angle** of the beam catcher was of interest because steeper cant angles reduce the cross sectional area of the bias plates (i.e. the non-sputtering surfaces) that is exposed to the beam. We therefore expected the optimizer to converge to the minimum cant angle possible. This served to validate the optimizer's operation, though would not provide meaningful insight into the optimal angle for mitigating ion backstreaming.

In our first set of optimization studies, we allowed all three parameters to be free. In these simulations, the optimizer converged to the minimum cant angle (as expected), a gap width of zero, and to a range near the thruster (though not at the minimum limit). Nelder-Mead optimization yielded a range of 1.24 m. Gaussian process regression yielded a range of 1.37 m. Both exceeded the minimum range limit (which was below 1.0 m), thereby implying that backsputter production by the support structure dominates at extremely near ranges. The gap width convergence to zero implies that any amount of shadow shielding provided by the beam catchers is negated by backsputter transport through the gap between the plates.

In our second set of optimization studies, we set the gap distance to zero and swept only the range. To set the angle, we assumed the beam catcher's backstreaming ion beam to have an 18° divergence angle and used the range to calculate the cant angle that would obtain a 0.66 m wide ion-free window centered at the thruster. Figure 8a shows a screenshot of the beam catcher configured in one of these simulations. These studies examined the effect of steeper cant angles being necessarily required to deflect ions at closer ranges. We note that 18° was a value physically motivated by unpublished data taken after the conclusion of testing by Hurley.[10]

Figure 8b shows results from the second set of optimization studies. A clear optimum range of 1.6-1.8 m is visible. The conclusion of these simulations was that to attain maximum backsputter reduction, the beam catcher should be configured such that: there is no gap between the panels; the forward tower is placed between 1.6 and 1.8 meters from the thruster; and the cant angle is as shallow as possible.

B. Langmuir Probe (LP) Analysis

We used a Langmuir probe to measure the plasma potential, V_p, near the QCM. To obtain the plasma potential with uncertainty we used the Markov Chain Monte Carlo inference algorithm to learn the parameters of two lines fit to the inverse temperature and electron saturation regions of the probe trace and calculating the intersection of the lines. The procedure we followed in processing each probe trace was:

1. Identify the probe floating voltage, V_f, as the voltage where the current draw is zero and the ion saturation current, $I_{sat} < 0$, as the minimum current value in the trace.
2. Extract the portion of the I-V trace where $V > V_f$ and shift the corresponding currents up by I_{sat}.
3. Take the natural logarithm of the extracted and shifted trace.
4. Fit lines to the last 30% of data points and to the first 5-10% of data points using the Markov Chain Monte Carlo (MCMC) algorithm to obtain 1500 samples of the posterior distributions of the slopes and y-intercepts for each line.
5. Using the slope and y-intercept samples obtained by MCMC, for each sample, compute the voltage where the lines intersect to thereby obtain samples over the posterior distribution of the intersection points.
6. Compute the mean of the intersection voltage sample set to be V_p.
7. Obtain a 95% confidence interval by computing the 2.5th and 97.5th percentile values of the voltage sample set. The error bars thus represent the voltage band over which we are 95% confident that the true plasma potential, V_p, lies within.

Figure 11 shows an example fit to data processed through step 3 of the above algorithm. We note that it is typical to take the additional step of subtracting the cathode to ground voltage from V_p to obtain the plasma potential with respect to the cathode. This is done because Langmuir probe measurements are taken with respect to (w.r.t.) facility ground and the potential difference between the plasma and cathode is a typical metric of interest in evaluating electric propulsion systems. We did not make this correction here because we were interested in obtaining the plasma potential w.r.t. facility ground.

C. Retarding Potential Analyzer (RPA) Analysis

We used a retarding potential analyzer to measure the ion energy distribution functions of backstreaming ions. Measuring RPA collector current while sweeping the filtering grid bias returns an I-V trace that represents the cumulative density function (CDF) of ions by energy level. The derivative of this trace is the probability density function (PDF) of ion energies. In the beam catcher plume, the PDF exhibits two peaks, one at a low voltage (near the plasma potential) and one at a high voltage (near the bias voltage of beam catcher). These peaks correspond to two distinct populations of ions, one with low energy (background plasma) and one with high energy (backstreaming ions). The high energy population is of particular interest because we believe that this population is responsible for sputtering at the surface of the QCM. Hence, it is valuable to obtain estimates for the most probable energy of the high energy population of ions. For convenience, we note that ion energy is given by $E = q\phi$ where ϕ is the voltage through which the ion is accelerated. Assuming singly charged ions from the beam catcher, $E = \phi$, and we can thus use the terms most probable *energy* and most probable *voltage* interchangeably.

To obtain the most probable voltage of each population, we fit a dual error function (the sum of two error functions) directly to the data obtained by the RPA. Specifically, we represent the RPA trace by the function

$$RPA(V) = \frac{A_1}{2}\left[1 - \text{erf}\left(\frac{V - V_{0,1}}{\sqrt{2}\sigma_1}\right)\right] + \frac{A_2}{2}\left[1 - \text{erf}\left(\frac{V - V_{0,2}}{\sqrt{2}\sigma_2}\right)\right] + C, \quad (1)$$

where we must fit amplitude parameters A, variance parameters σ and centering parameters V_0 for each population $\{1, 2\}$, as well as a vertical offset parameter C (which is nominally zero). The most probable voltage of each population are the centering parameters, $V_{0,1}$ and $V_{0,2}$. This mathematical representation is valid because the ion energy distribution function (the PDF) is bi-Maxwellian, one Maxwellian corresponding

to each of the low and high energy ion populations. The integral of this function (the CDF, which is directly measured by the RPA) is therefore the sum of two error functions.

The advantage of fitting a dual error function directly to the RPA data is that it avoids the smoothing, filtering, and numeric differentiation steps necessary to fit Maxwellians to the derivative of the RPA data. In this way, we remove uncertainties associated with pre-processing the data and can directly employ MCMC sampling to obtain uncertainties over the most probable voltages. The procedure we followed to process each trace was:

1. Clean outliers from the raw RPA trace.
2. Use MCMC to obtain 2000 samples from the posterior distribution of the dual error function variables A_1, A_2, $V_{0,1}$, $V_{0,2}$, σ_1, σ_2, and C per Eq. 1.
3. Compute the means of the samples for $V_{0,1}$ and $V_{0,2}$ to be the most probable voltage for each population.
4. Obtain a 95% confidence interval for each most probable voltage by computing the 2.5th and 97.5th percentile values of each voltage sample set.

Figure 12 shows an example fit of Eq. 1 to RPA data. In that figure, the curve shown is the curve corresponding to the mean values of each of the seven fit parameter sample sets.

D. Eckstein Curve Fitting

The sputter yield curve is a model for describing the number of sputterants released from a target surface as a function of bombarding ion energy. Eckstein[16] introduces a semi-empirical model that is commonly used in the electric propulsion field.[14,20,21] This model is given by

$$Y(E) = Q s_n \frac{\left(\frac{E}{E_{th}} - 1\right)^{\mu}}{\frac{\lambda}{w} + \left(\frac{E}{E_{th}} - 1\right)^{\mu}}, \tag{2}$$

where Y is sputter yield in units of atoms/ion, E is the incident ion energy, and $\{Q, \lambda, \mu, E_{th}\}$ are empirical fit parameters. The other values in this formula are w and s_n. The parameter s_n is the reduced nuclear stopping power which Yim[14] says is best represented by the Krypton-Carbon (KC) potential at low energies. This formula is

$$s_n^{KC} = \frac{0.5 \ln(1 + 1.2288\epsilon)}{\epsilon + 0.1728\sqrt{\epsilon} + 0.008\epsilon^{0.1504}},$$

where ϵ is the reduced energy. The value w is also a function of the reduced energy,

$$w = \epsilon + 0.1728\sqrt{\epsilon} + 0.008\epsilon^{0.1504}.$$

The reduced energy is given by

$$\epsilon = \frac{a_L}{Z_i Z_s} \frac{4\pi\varepsilon_0}{e^2} \frac{M_s}{M_i + M_s} E,$$

where Z_i and Z_s are the atomic numbers of the ion and surface elements, respectively, and M_i and M_s are the atomic weights of the ion and surface elements in units of [g/mol]. The Lindhard screening length, a_L, is given by,

$$a_L = \left(\frac{9\pi^2}{128}\right)^{1/3} a_0 \left(Z_i^{2/3} + Z_s^{2/3}\right)^{-1/2},$$

where $a_0 = 0.529\mathring{A}$ is the Bohr radius. The model requires that the four fit parameters $\{Q, \mu, \lambda, E_{th}\}$ be learned from data. Q, μ, and λ possess little physical significance. The threshold energy, E_{th}, represents the minimum energy required to initiate sputtering off a surface. Yim[14] notes that E_{th} "is difficult to assess experimentally or analytically, yet strongly influences the curve fits."

There is scarce literature for the bombardment of noble gases on monatomic materials at low energies, which has posed a substantial challenge for the electric propulsion community.[14] Xenon-carbon sputter yields have been characterized by the community at low (< 1 kV) ion energies[13,14] due to the historical

prevalence of xenon as a propellant. However, there do not exist detailed characterizations for argon-carbon, or argon-steel sputter yields, both of which are significant to this work.

To obtain relevant sputter yield curves, we use the Bayesian inference Markov Chain Monte Carlo (MCMC) method for inferring the fit parameters from data with uncertainty. The data we use comes from a textbook by Behrisch and Eckstein[16] in which they collate data for many combinations of ion and surface materials from the periodic table up to tens of kilovolts of incident ion energies. We extracted data for argon-carbon bombardment below 600V and for argon-iron bombardment below 1 kV and used MCMC to infer each of the four fit parameters. Figure 30 shows curve fits shown alongside the data used for the fits. Although our argon-carbon fit appears to underpredict the sputter yield of graphite below 200V, our threshold energy agrees with the xenon-carbon threshold energy found by Yim.

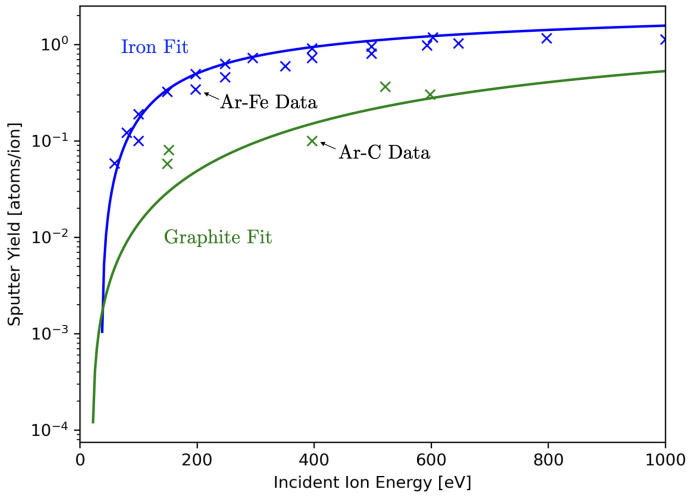

Figure 30: Eckstein curve fits for argon ions with data. The curves are plotted using the most probable value for each fit parameter.

E. Witness Plate Photos

In Study 2, seven sets of witness plates were installed in a row above the thruster. Each set consisted of a grounded aluminum plate immediately adjacent to an acrylic plate. The plate sets were labeled A-G. The centerline of plate A was in line with thruster centerline. The plates were equally spaced by 8.7 cm (3.5”), spanning a total length of 52 cm. The plates were installed on the side of the thruster corresponding to the nearer beam tower. Figure 22 shows before and after photos of the entire row of plates. Here, we show close-up photos for each lettered plate set.

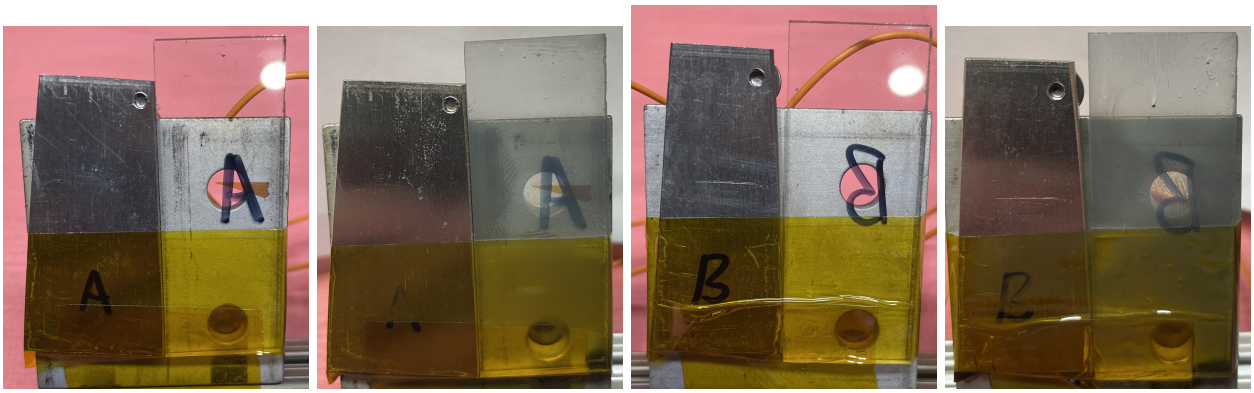

(a) A before. (b) A after. (c) B before. (d) B after.

Figure 31: Witness plate sets A and B.

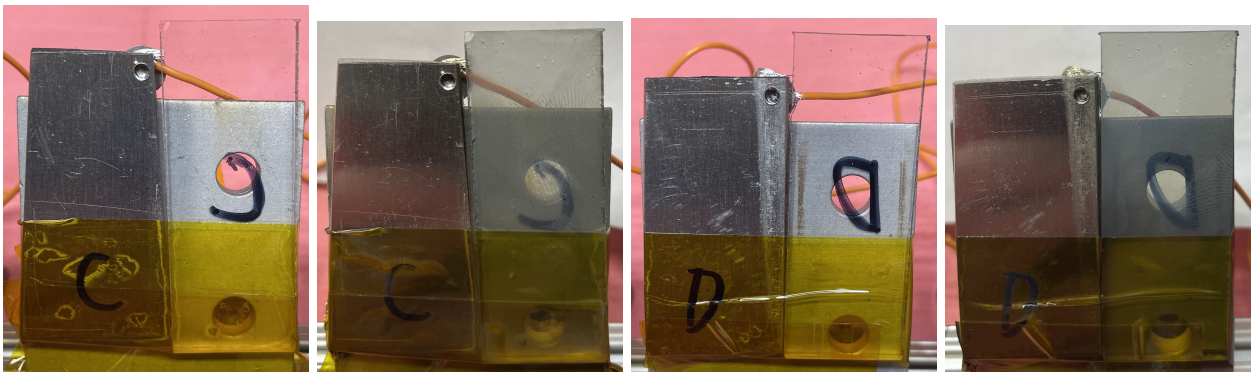

(a) C before. (b) C after. (c) D before. (d) D after.

Figure 32: Witness plate sets C and D.

(a) E before. (b) E after. (c) F before. (d) F after.

Figure 33: Witness plate sets E and F.

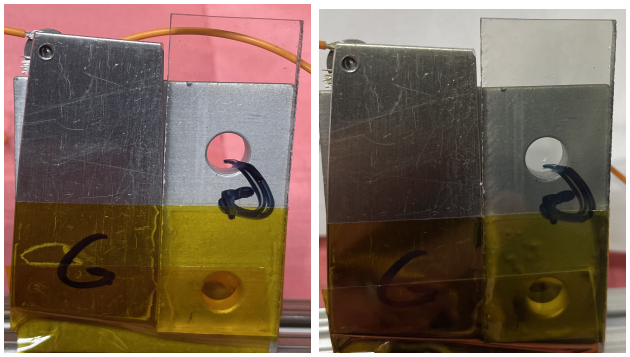

(a) G before. (b) G after.

Figure 34: Witness plate set G.

References

[1]Benjamin Jorns, Christopher A Dodson, John R Anderson, Dan M Goebel, Richard R Hofer, Michael J Sekerak, Alejandro Lopez Ortega, and Ioannis G Mikellides. Mechanisms for pole piece erosion in a 6-kw magnetically-shielded hall thruster. In *52nd AIAA/SAE/ASEE Joint Propulsion Conference*, page 4839, 2016.

[2]Matthew P Byrne, Parker J Roberts, and Benjamin A Jorns. Coupling of electrical and pressure facility effects in hall effect thruster testing. *meta*, 5:2, 2006.

[3]Robert B Lobbia et al. Accelerating 23,000 hours of ground test backsputtered carbon on a magnetically shielded hall

thruster. In *AIAA Propulsion and Energy 2019 Forum*, page 3898, 2019.

[4]Jason D Frieman, Hani Kamhawi, Wensheng Huang, Jon Mackey, Drew M Ahern, Peter Y Peterson, James H Gilland, Scott J Hall, Richard R Hofer, Derek Inaba, et al. Wear test of the 12.5-kw advanced electric propulsion system engineering test unit hall thruster. In *AIAA Propulsion and Energy 2020 Forum*, page 3625, 2020.

[5]Rohit Shastry et al. Status of nasa's evolutionary xenon thruster (next) long-duration test as of 50,000 h and 900 kg throughput. In *International Electric Propulsion Conference (IEPC2013)*, number IEPC-2013-121, 2015.

[6]Ioannis G Mikellides, Alejandro Lopez Ortega, and Benjamin Jorns. Assessment of pole erosion in a magnetically shielded hall thruster. In *50th AIAA/ASME/SAE/ASEE Joint Propulsion Conference*, page 3897, 2014.

[7]Jerold Emhoff and Iain Boyd. Grid erosion modeling of the next ion thruster optics. In *39th AIAA/ASME/SAE/ASEE Joint Propulsion Conference and Exhibit*, page 4868, 2003.

[8]Leanne L Su, Parker J Roberts, Tate Gill, William Hurley, Thomas A Marks, Christopher L Sercel, Madison Allen, Collin B Whittaker, Matthew Byrne, Zachariah Brown, et al. Operation and performance of a magnetically shielded hall thruster at ultrahigh current densities on xenon and krypton. In *AIAA SCITECH 2023 Forum*, page 0842, 2023.

[9]Seth J Thompson, Jack Garman, Zach C Robertson, John D Williams, William Hurley, Tate Gill, Collin B Whittaker, and Benjamin Jorns. Methods for mitigating backsputter in electric propulsion test facilities i: Beam halter concept and design. In *AIAA SCITECH 2024 Forum*, page 2367, 2024.

[10]William J. Hurley, Camber Hortrop, Collin B. Whittaker, Tate M. Gill, Christopher May, and Benjamin A. Jorns. Methods for mitigating backsputter in electric propulsion test facilities ii: Beam halter demonstration during hall thruster testing (upcoming). In *AIAA SCITECH 2024 Forum*, 2024.

[11]Braden Oh, William Hurley, Grace Zoppi, Christopher May, Collin Whittaker, and Benjamin Jorns. Carbon backsputter mitigation with a retarding beam dump. In *38th International Electric Propulsion Conference*, 2025.

[12]Eric A Viges, Benjamin A Jorns, Alec D Gallimore, and JP Sheehan. University of michigan's upgraded large vacuum test facility. In *36th International Electric Propulsion Conference*, pages 1–18, 2019.

[13]John Williams, Mark Johnson, and Desiree Williams. Differential sputtering behavior of pyrolytic graphite and carbon-carbon composite under xenon bombardment. In *40th AIAA/ASME/SAE/ASEE Joint Propulsion Conference and Exhibit*, page 3788, 2004.

[14]John T Yim. A survey of xenon ion sputter yield data and fits relevant to electric propulsion spacecraft integration. In *International Electric Propulsion Conference (IEPC)*, number GRC-E-DAA-TN45154, 2017.

[15]Thomas Marks. Sputterer. `https://github.com/archermarx/Sputterer/`, 2024.

[16]Rainer Behrisch and Wolfgang Eckstein. *Sputtering by particle bombardment: experiments and computer calculations from threshold to MeV energies*, volume 110. Springer Science & Business Media, 2007.

[17]Chih-Shun Lu and Owen Lewis. Investigation of film-thickness determination by oscillating quartz resonators with large mass load. *Journal of Applied Physics*, 43(11):4385–4390, 1972.

[18]James H Gilland, George Williams, Jonathan M Burt, and John Yim. Carbon back sputter modeling for hall thruster testing. In *52nd AIAA/SAE/ASEE Joint Propulsion Conference*, page 4941, 2016.

[19]Joshua Rovey, Mitchell Walker, Peter Peterson, and Alec Gallimore. Evaluation of a magnetically filtered faraday probe for measuring the ion current density profile of a hall thruster. In *40th AIAA/ASME/SAE/ASEE Joint Propulsion Conference and Exhibit*, page 3948, 2004.

[20]Mackenzie Meyer, Matthew Byrne, Benjamin Jorns, and Iain D Boyd. Erosion of a meshed reflector in the plume of a hall effect thruster, part 1: Modeling. In *AIAA Propulsion and Energy 2019 Forum*, page 3987, 2019.

[21]Keita Nishii, Sean Clark, Joshua Tompkins, Nakul Nuwal, Deborah A Levin, and Joshua L Rovey. Numerical simulation of carbon sputtering for electric propulsion in the ground facility. In *37th International Electric Propulsion Conference Massachusetts Institute of Technology, Cambridge, MA, USA, IEPC-2022*, volume 379, 2022.